Ultrasound and Microbubble-Induced Nanoparticle Delivery and Inflammatory Response in Ischemic Mouse Skeletal Muscle

---

A Thesis

Presented to

the faculty of the School of Engineering and Applied Science

University of Virginia

---

in partial fulfillment

of the requirements for the degree

Master of Science

by

Judith Hsiang

August

2014

APPROVAL SHEET

The thesis

is submitted in partial fulfillment of the requirements

for the degree of

Master of Science

AUTHOR

The thesis has been read and approved by the examining committee:

Dr. Richard Price

Advisor

Dr. John Hossack

Dr. Alexander Klibanov

Accepted for the School of Engineering and Applied Science:

Dean, School of Engineering and Applied Science

August

2014

ACKNOWLEDGEMENTS

My deepest gratitude is to my advisor, Dr. Richard Price, for providing me with the extraordinary opportunity to explore biomedical research and for giving me invaluable guidance and support throughout these years with incredible patience. I owe my thanks to Dr. Alexander Klibanov and Dr. John Hossack for their valuable advice over the years. In particular, my research would not have been possible without the help of Dr. Klibanov, who provided microbubbles constantly ever since I began as an undergraduate.

I must thank all the members of the Price lab from the past and present for making this a great and memorable experience. I especially thank Ji Song, Josh Meisner, and Caitlin Burke for their advice and help in all aspects of research. To the undergraduate student volunteers I worked with over the years I owe my thanks for their help with countless hours of data collection, especially Jacqueline Niu.

My sincerest thanks also go to Linsey Phillips from the Hossack Lab, Sunil Unnikrishnan from the Klibanov Lab, and Yuhling Wang and Jose Tlaxca from the Lawrence Lab for their generous assistance and insightful discussions.

To my friends and family, I whole-heartedly thank them for their encouragement and unconditional support during the ups and downs, for keeping me sane when the light at the end of the tunnel was approaching much too quickly, and for helping me hold things together all the way to the finish line when my world turned upside down.

TABLE OF CONTENTS

ABSTRACT

Peripheral arterial occlusive disease is a major health problem worldwide. Patients diagnosed with more advanced stages of the disease face very poor prognosis and have limited treatment options. To this end, therapeutic vascular remodeling approaches facilitated by ultrasound and microbubble-mediated therapeutics studied have been developed with encouraging outcomes and demonstrated possibilities of being translated into more targeted and non-invasive therapies. This research sought to explore and examine the therapeutic agent delivery potential and bioeffects of the ultrasound-microbubble treatment modality in a peripheral arterial occlusive disease mouse model to serve as reference for future therapeutic vascular remodeling studies. In particular, this project aimed to determine how ultrasound peak negative pressures of 0.7 MPa, 0.55 MPa, 0.4 MPa and 0.2 MPa affect the distribution of nanoparticles delivered and the inflammatory response generated by ultrasound-microbubble interactions in ischemic mouse skeletal muscle. For studying nanoparticle delivery, 50 nm and 100 nm particles were introduced into mice either through femoral artery cannulations or jugular vein cannulations. For the femoral artery route, increased PNP resulted in increased delivery mostly to the interstitium for both nanoparticle sizes, whereas for the jugular vein route there was increased 50 nm nanoparticle delivery mostly to the endothelium as pressure increased up to 0.55 MPa. It was concluded that in coordination with microbubble concentration and size distribution, adjusting the peak negative pressure applied could be a feasible approach for improving the targeting specificity of NP delivery into the tissue. For studying inflammatory response, CD45+ cells were quantified in ultrasound-microbubble-treated muscle cross sections. The results implied no significant differences across the ultrasound peak negative pressures applied.

LIST OF FIGURES

LIST OF TABLES

NOMENCLATURE

ANOVA:	Analysis of Variance
BSA:	Bovine Serum Albumin
CLI:	Critical Limb Ischemia
GM:	Gracilis Muscle
I.P.:	Intraperitoneal
LDPI:	Laser Doppler Perfusion Imaging
MB:	Microbubble
MBs:	Microbubbles
MHz:	megaHertz
NP:	Nanoparticle
NPs:	Nanoparticles
OCT:	Optimal Cutting Temperature compound
PAOD:	Peripheral Arterial Occlusive Disease
PBS:	Phosphate Buffered Saline
PE-10:	Polyethylene 10
PFA:	Paraformaldehyde
PNP:	Peak Negative Pressure
PNPs:	Peak Negative Pressures
ROI:	Region of Interest
US:	Ultrasound
US-MB:	Ultrasound-Microbubble
USMB:	Ultrasound and Microbubble

USMBs: Ultrasound and Microbubbles

USMB-NP: Ultrasound and Microbubble-Mediated Nanoparticle Delivery

UMTD: Ultrasound and Microbubble-Targeted Delivery

VEGF: Vascular Endothelial Growth Factor

CHAPTER 1: INTRODUCTION

1.1 MOTIVATION AND OVERVIEW

Peripheral arterial occlusive disease (PAOD) is a major healthcare problem worldwide, affecting approximately 27 million people in Europe and North America (Harris, 2008) and 8 million in the United States alone (Roger et al., 2011). Patients diagnosed with more advanced stages of the disease, known as critical limb ischemia (CLI), face very poor prognosis. Approximately 500 to 1000 people per million per year worldwide develop CLI (Clement, 2008), 40 – 60% of those diagnosed undergo amputation while the remainder endure invasive and comprehensive treatments limited to transluminal angioplasty or surgical revascularization (Palmer-Kazen, Wariaro, Luo, & Wahlberg, 2004). Unfortunately, many CLI patients are poor candidates for either intervention (Bobek, Taltynov, Pinterova, & Kolostova, 2006). To this end, alternative remedies such as therapeutic arteriogenesis and angiogenesis that are less invasive have been developed with encouraging outcomes. Moreover, in combination with research advancement in ultrasound and microbubble-mediated therapeutics over the last two decades, therapeutic angiogenesis/arteriogenesis approaches studied have demonstrated possibilities of being translated into more targeted and non-invasive methods. This research sought to explore and examine the therapeutic agent delivery potential and bioeffects of the ultrasound-microbubble treatment modality in a PAOD mouse model to serve as reference for future therapeutic vascular remodeling studies.

1.2 PERIPHERAL ARTERIAL OCCLUSIVE DISEASE

Peripheral arterial occlusive disease (PAOD), also known as peripheral artery disease and peripheral vascular disease, is a highly prevalent condition that can result from acute trauma, thrombosis, embolisms, vasculitis, atherosclerosis or inflammatory processes leading to arterial

stenosis (Clement, 2008; Harris, 2008; Wood & Hiatt, 2001; Ziegler 2010). In the more advanced stages of the disease where limbs have become chronically ischemic (i.e. critical limb ischemia), with the existing invasive treatment options of transluminal angioplasty or surgical revascularization, 1 year after diagnosis approximately 25% of patients will have died while 30% will have undergone major amputation (Clement, 2008); 15 years after diagnosis, only 30% will remain alive (Harris 2008). PAOD is common among the elderly, hence with the worldwide demographic continuing to age, the prevalence of PAOD will likely increase dramatically over the next 20 years. Furthermore, cardiovascular diseases including PAOD that were once associated with industrialized nations are now emerging or rapidly increasing in developing countries (A. Boutayeb & Boutayeb, 2005). Thus, there is clearly a pressing need for less invasive and more effective therapeutic strategies.

1.3 THERAPEUTIC VASCULAR REMODELING

Therapeutic vascular remodeling involves stimulating angiogenesis, the sprouting of new capillaries from pre-existing vessels, and/or arteriogenesis, the growth of functional collateral arteries from pre-existing arterio-arteriolar anastomoses (Heil, Eitenmüller, Schmitz-Rixen, & Schaper, 2006). In response to the need for less invasive and more effective treatments for PAOD, therapeutic vascular remodeling conducted through cell-, gene-, and protein-based interventions have been broadly explored. Studies include, for example, implanting peripheral blood mononuclear cells (Iba et al., 2002), endothelial progenitor cells (Kalka et al., 2000) or adipose tissue-derived stromal cells (Nakagami, 2005) into ischemic animal hindlimbs to promote vascular remodeling; transfecting native cells in ischemic limbs to locally overexpress growth factors from genes/plasmids encoding for vascular endothelial growth factor (Tsurumi et al., 1996) or hepatocyte growth factor (Taniyama et al., 2001), factors known to be critically

involved in the vascular remodeling process (Bobek, Taltynov, Pinterova, & Kolostova, 2006); and delivering growth factors or cytokines essential for angio/arteriogensis directly to the ischemic tissue (Henry, 2003; Van Royen et al., 2002).

And while numerous pre-clinical studies and pilot/small open-labeled trials of cell-, gene-, and protein-based interventions have demonstrated promotion of vascular remodeling and tissue reperfusion, there have also been harmful complications and insignificant clinical outcomes observed in pre-clinical experiments and larger double-blinded randomized placebo-controlled trials (Epstein, Kornowski, Fuchs, & Dvorak, 2001; Kaplan, Palmer, Bekeredjian, & Shohet, 2004; Losordo & Dimmeler, 2004; Mughal, Russell, Ponnambalam, & Homer-Vanniasinkam, 2011). One possible explanation for these unfavorable results could be the suboptimal delivery of therapeutic agents to target cells or tissues (Kobulnik, Kuliszewski, Stewart, Lindner, & Leong-Poi, 2009).

1.4 Ultrasound and Microbubble-Facilitated Therapeutic Delivery

The use of ultrasound (US) in combination with circulating microbubble (MB) contrast agents to enhance targeted interventions *in vivo* was suggested around two decades ago (Klibanov, 2006), and since then ultrasound-microbubble interactions have been widely utilized in research for its ability to facilitate the delivery, i.e. ultrasound and microbubble-targeted delivery (UMTD), of genetic material, protein and chemotherapeutic agents in a non-invasive, localized and targeted manner (Pitt, Husseini, & Staples, 2004) in numerous tissues for various diseases. For example, US-MB interactions have been used to promote the delivery of hepatocyte growth factor genes into the myocardium for treatment of acute myocardial infarction (Kondo et al., 2004), the delivery of fibroblast growth factor-2 to the hindlimb skeletal muscle for therapeutic arteriogenesis (Chappell, Song, Burke, Klibanov, & Price, 2008a), and the

transfer of doxorubicin through the blood brain barrier into the central nervous system for investigating brain tumor treatments (Treat et al., 2007). In comparison to the conventional intraarterial, intravenous, and intramuscular methods for drug and gene delivery, UMTD seems to have become more attractive as the mode of agent transport in disease treatment investigations, including those in therapeutic vascular remodeling. Possible reasons are that intraarterial and intravenous injections could result in more systemic delivery of genes or growth factors to non-targeted tissue and lower transfection efficiency (Kornowski, Fuchs, Leon, & Epstein, 2000) or induce more vascular alterations at unintended sites (Epstein, Kornowski, Fuchs, & Dvorak, 2001). Intramuscular delivery is limited by treatment applied to only around the injection site and hence the probable need for several injections, its inability to target specific cell types, and its impracticality of repetitive treatments in certain tissues such as the heart (Kobulnik et al., 2009). On the contrary, UMTD can deliver therapeutic agents to intended cells and tissue regions with limited undesirable systemic transfers as agent transport driven by the US-MB interactions occur mostly in zones exposed to US. The US-MB interactions *in vivo* cause temporarily enhanced permeability of cell membranes and microvascular walls, which allow for less obstructed travel of promising intravascular drug carriers such as liposomes and microspheres that have diameters commonly exceeding 100 nm (Price & Kaul, 2002). The extent of such bioeffects generated from US-MB interactions can be selectively modulated by adjusting the US and MB parameters applied, including for example the US center frequency (Miller & Chunyan, 2004; Miller, 2007; Nyborg, 2007), US peak negative pressure, pulse length (Tu, Matula, Brayman, & Crum, 2006), pulse interval (Samuel, Cooper, Bull, Fowlkes, & Miller, 2009; Song et al., 2002), MB concentration (Miller & Quddus, 2000; Song, Klibanov, Hossack, & Price, 2008) and MB size distribution (Caskey, Stieger, Qin, Dayton, & Ferrara, 2007). The

noninvasive nature of UMTD permits better toleration of recurring treatments necessary. Additionally, MBs could carry therapeutic agents within the gas core, bubble shell or on the shell surface (Klibanov, 2006) that are released as the bubbles are disrupted upon US exposure, which could contribute to greater payload transported at the targeted site (Burke, Hsiang, Alexander, Klibanov, & Price, 2011). The attachment of specific ligands to the bubble shell could facilitate selective binding of payload-carrying MBs to certain cell receptors, which would also allow for more delivery at a higher level of targeting specificity and also minimize the systemic loss of agents and transfer to unintended regions (Klibanov, 2006; Lum et al., 2006). These favorable attributes have made UMTD strongly preferable, and have therefore attracted wide spread research attention aimed at exploring its capacity to improve therapeutic outputs for assorted diseases and also better understanding of its functional mechanisms.

Based on the consistencies that have emerged from *in vitro* and *in vivo* studies examining US-MB interactions and the associated bioeffects by testing various permutations of ultrasound exposure parameters, bubbles, cells, and tissues, it seems that USMB-directed therapeutic delivery is likely facilitated via the inertial and/or noninertial cavitation of MBs by US. For inertial cavitation, formerly called transient cavitation, delivery is driven by US causing MBs to expand and contract non-linearly and asymmetrically collapse when near cells. During such a violent collapse, the surrounding liquid rushes inward in a non-uniform manner that forms a liquid jet, which could pierce through endothelial cell membranes or across vessel walls to create transient pores that allow for agent distribution by convection (Caskey et al., 2007; Nyborg, 2007; Prentice, Cuschieri, Dholakia, Prausnitz, & Campbell, 2005; Price & Kaul, 2002; Price, Skyba, Kaul, & Skalak, 1998). This sonoporation phenomenon could also possibly be generated from penetration by bubble shell fragments post bubble collapse (Chappell & Price, 2006; Fan,

Kumon, Park, & Deng, 2010). Additionally, violent collapses of microbubbles are also known to produce shock waves, heat, and free radicals that may possibly alter cellular and vascular permeability (Chappell et al., 2006; Miller et al., 2008; Mitragotri, 2005). However, for microbubbles such as Optison® where the encapsulated perfluorocarbon gas has high heat capacity, the production of free radicals is greatly reduced and the maximum temperature produced during MB collapse is also much less for such gases than air (Nyborg, 2007). In fact, it has been shown that free radicals play an insignificant role in USMB-enhanced delivery of genes to vascular cells with Optison® as the choice for MBs (Lawrie et al., 2003). Noninertial cavitation, formerly termed stable cavitation, involves the stable oscillations of MBs driven by US below the inertial cavitation threshold. The oscillating MBs exert mechanical stresses on cells and vessels by either directly pushing or pulling against it (Caskey et al., 2007; van Wamel, Bouakaz, Versluis, & de Jong, 2004a; van Wamel, Bouakaz, Versluis, & de Jong, 2004b) or through microstreaming – small-scale steady circulatory flow in the immediate vicinity of a vibrating bubble – in proximity to the endothelium (Collis et al., 2010; Liu & Wu, 2008; Stride, 2009). Such stresses seem to generate transient intercellular gaps and cell membrane pores (Juffermans et al., 2009; Meijering et al., 2009; van Wamel et al., 2006), and also stretch-activate cell membrane receptors and ion channels that trigger downstream signaling to promote endocytosis or alter membrane barrier properties (Meijering et al., 2009; Tran, Le Guennec, Bougnoux, Tranquart, & Bouakaz, 2008), which allow for greater delivery of therapeutic agents into targeted regions.

Given the diversity of biophysical mechanisms associated with varying levels of cavitation in UMTD, we were intrigued by the possibility of harnessing the associated bioeffects

in a more selective manner via varying the US and MB parameters applied to further explore and refine the targeted therapeutic capacity of UMTD.

1.5 Ultrasound and Microbubble-Induced Nanoparticle Delivery and Inflammatory Response

Among the US and MB parameters known to influence the extent of cavitation-generated bioeffects, we were interested in learning about the impact of varying the US peak negative pressure (PNP) applied. In particular, this research investigated the effects on nanoparticle (NP) delivery and inflammatory response in the ischemic mouse skeletal muscle.

In previous UMTD work presented by our group, when 100 nm fluorescent polystyrene particles were successfully delivered into the targeted skeletal muscle, particles were observed both in the interstitial and endothelial spaces (Chappell et al., 2008a). For therapeutic vascular remodeling and likely many other treatment applications, more precise agent delivery, such as to only the interstitium or only the endothelium, could be very beneficial. For therapeutic vascular remodeling via gene therapy for instance, it would be advantageous to transfect only the myocytes surrounded by interstitial spaces or only the endothelial cells in the endothelium with the corresponding genetic materials to express specific proteins involved in the remodeling process. And concerning gene delivery especially, this improvement in transport precision could be a welcoming improvement to the prohibitively inefficient transfection efficiencies often seen in intravascular non-viral gene delivery systems. Therefore, our aim was to determine whether NP distribution across endothelial and interstitial spaces in the muscle would change in response to a range of US PNP levels applied.

UMTD can be a rather violent process. The same cavitation levels that are required to promote agent delivery into cells and tissues through perforations or permeability changes can also have adverse effects including cell death, hemorrhage, and inflammation, which may not be

eliminated entirely in the interest of therapeutic gain. For vascular remodeling, UMTD-induced inflammation may not be entirely unwanted since the inflammatory cells involved play key roles and aid remodeling processes (Yoshida et al., 2005). However, in conditions where the UMTD-directed therapeutic consequences of certain drugs or genes are studied, in the interest of more customized and controlled UMTD treatments, and/or in other treatment applications such as for cancer where inflammation may intensify disease severity (Balkwill & Mantovani, 2001; Ono, 2008), it would be valuable to minimize inflammation. Hence, our goal was to obtain a profile of the inflammatory response in the muscle upon USMB application with various input levels of US PNPs.

Overall, a better understanding of how various US PNP levels affect USMB-induced nanoparticle delivery and inflammatory response in ischemic mouse skeletal muscle will serve as a valuable reference for devising more refined UMTD approaches for therapeutic vascular remodeling and many other disease treatments.

1.6 OBJECTIVES

There are two main objectives to this project. First, to determine how various ultrasound peak negative pressures applied affect the distribution of nanoparticles delivered by ultrasound-microbubble interactions in ischemic mouse skeletal muscle (Chapter 5). Second, to measure the inflammatory response generated by ultrasound-microbubble interactions in ischemic mouse skeletal muscle with various levels of ultrasound peak negative pressures applied (Chapter 6).

To meet the two objectives described above, a number of studies were conducted in preparation. Specifically, a peripheral arterial occlusive disease mouse model for studying therapeutic vascular remodeling facilitated by ultrasound and microbubble-targeted delivery was established (Chapter 2), a functional ultrasound-mediated microbubble destruction protocol on

the disease model was developed (Chapter 3), and the ultrasound and microbubble delivery systems were characterized for obtaining the specific input voltages necessary to output desired ultrasound peak negative pressures and for gaining more accurate information on the microbubble population delivered (Chapter 4).

CHAPTER 2: ESTABLISHMENT OF THE ISCHEMIC MOUSE HINDLIMB MODEL

2.1 INTRODUCTION

A suitable peripheral arterial occlusive disease (PAOD) model is necessary to investigate the effects of therapeutic vascular remodeling facilitated by ultrasound and microbubble-targeted delivery. In particular, the model requires significant ischemia post vessel occlusion and slow recovery for several days subsequently to serve as a treatment window. Popular POAD models include those such as the hindlimbs of C57BL/6 and BALB/c mice. Compared to C57BL/6 mice, BALB/c mice have fewer native collateral vessels with poorer ability to remodel after obstruction upstream (Chalothorn & Faber, 2010; Helisch et al., 2005), which gives the two strains distinct ligation-recovery profiles. To this end, the hindlimbs of C57BL/6 and BALB/c were assessed for suitability for our studies.

Both strains of mice were first subjected to femoral artery ligations to create ischemic hindlimb conditions. The feet were then monitored afterwards for reperfusion using laser Doppler perfusion imaging (LDPI) to generate ligation-reperfusion (i.e. recovery) profiles for each strain. Furthermore, BALB/c gracilis muscle collateral vessel diameters were also quantified post ligation to verify the presence of significant vessel remodeling and hence the future use of the muscle as an experimental target for vascular remodeling studies. This quantification was not performed on the C57BL/6 strain, as its gracilis muscles had already been used as an experimental platform by our group for therapeutic arteriogenesis studies (Chappell et al., 2008a; Chappell, Song, Klibanov, & Price, 2008b).

2.2 EXPERIMENTAL METHODS

To generate ligation-reperfusion profiles for femoral artery-ligated C57BL/6 and

BALB/c mice (23 grams, 8 – 10 weeks old, Harlan Laboratories, Inc., Dublin, VA), laser Doppler imaging was done for several femoral artery-ligated mice of both strains during different experimental trials to maximize the use of each mouse. As a result, perfusion data gathered for each specific time point at pre-ligation, post-ligation, day 2, day 4…etc. was sourced from varying numbers of mice. See Table 2.1 (p. 19) for the exact number of mice from which data were collected for each time point. For collateral vessel diameter measurements in the BALB/c strain, 13 mice were used. See Table 2.2 (p. 21) for the specific number of mice used for each time point.

Mice in this study underwent a pre-ligation laser Doppler scan, femoral artery ligation and post-ligation laser Doppler scan on day 0, and then follow-up scans on a selection of days (including e.g. days 2, 4, 7, 10, 12, 14, 21) up until the day the gracilis muscles were harvested.

2.2.1 Femoral Artery Ligation

Mice receiving unilateral arterial occlusions were given the same initial preparations and maintained under sterile conditions throughout experimentation. Animals were anesthetized by an I.P. injection of ketamine (0.12 mg/g mouse), xylazine (0.012 mg/g mouse), and atropine sulfate (0.00008 mg/g mouse). Once the mice were under anesthesia, the eyes were covered with an ophthalmic ointment (Duratears, Alcon Laboratories, Inc., Forth Worth, TX) to prevent against light damage and dehydration. The inner thigh of each leg and the surrounding region were depilated and cleaned with a Betadine (Purdue Frederick Company, Norwalk, CT) wipe followed by an ethanol swab. The Betadine-ethanol cleaning sequence was then repeated 2 more times with short breaks of approximately 20 seconds in between to prevent the animal from becoming hypothermic.

If hindlimb perfusion was being monitored on the animal, laser Doppler imaging was done on the hindlimb regions of both legs prior to the Betadine-ethanol cleaning sequence. For details on the laser Doppler imaging process, see *2.2.2 Hindlimb Perfusion Monitoring.*

All surgical instruments were sterilized with high-pressure saturated steam at 121°C in an autoclave for around 35 minutes and allowed to cool before surgery. After the depilated area on the animal was cleaned, the animal was placed supine on a warmed surgical stage. A sterile drape covered the animal almost entirely, the inner thighs were exposed through openings in the drape and the nose and mouth were exposed at the edge of the drape. Viewing through a Zeiss surgical dissecting microscope (Stemi 2000, Carl Zeiss, Inc., Thornwood, NY), a skin incision less than 5 mm long was made on one leg directly along the femoral artery immediately distal to where the epigastric artery branches. The fascia and fat between the skin and underlying muscle were gently cleared by blunt dissection to expose the artery-vein pair running distal to where the epigastric artery-vein pair branches off of the femoral artery-vein. A separation of less than 4 mm in length was made between the artery and vein, sufficient for ligature placement. Special care was taken to leave the nerve running along this vessel pair intact and minimally disturbed. Two sterile pieces of silk sutures (6-0, Deknatel, Inc., Fall River, MA) were then tied at less than 2 mm apart around the separated section of the artery. The artery segment between the two ligatures was then severed with micro dissecting scissors. The skin incision was closed with sutures (5-0 Proline, Ethicon, Somerville, NJ) and the animal was left to recover on a heating pad. As the anesthesia wore off, an I.P. injection of buprenorphine (0.03 ml/animal, Reckitt Benckiser Pharmaceuticals Inc., Richmond, VA) was given, followed by a second dose 8-12 hours later.

2.2.2 HINDLIMB PERFUSION MONITORING

Hindlimbs were assessed for blood perfusion using an LDPI system pre-, post-ligation, and on desired days following throughout the remainder of the study. To perform laser Doppler imaging, the animal was anesthetized. For imaging pre- and post-ligation, the animal was anesthetized under the ketamine-xylazine-atropine mixture given in preparation for the femoral artery ligation detailed previously (see *2.2.1 Femoral Artery Ligation*). For imaging on days following ligation, the animal was anesthetized with ketamine (35mg/kg mouse) and dexmedetomidine (0.25mg/kg mouse) instead. The feet were cleaned and inner thighs of both legs were depilated. The animal was placed supine on a non-reflective light-absorbing black rubber pad and its feet were adhered to the rubber surface with double-sided masking tape. For convenience and accuracy in analysis, it was important that the masking tape was trimmed to a size where it was completely concealed by the feet in aerial view. The animal on the rubber pad was then placed onto a heating pad within a dark Plexiglas® box with a side opening and scanned using the LDPI system PeriScan (Perimed, Inc., Sweden) with accompanying software LDPIWin (Perimed Inc., Sweden). With the PeriScan scanner fixed at approximately 20 cm above the hindlimb region, scanning was performed with the specific settings of color scale at 0 Volt minimum and 10 Volt maximum, with amplification of 2x (see *Appendix A.* for more detail) at the high resolution setting. Upon completion of the scan, the animal was taken out of the box and removed from the rubber pad to recover on a heating pad. A subcutaneous injection of atipamezole (0.0006mg to 0.001mg per g of mouse) was then given to reverse the effect of dexemedetomidine.

2.2.3 *Hindlimb Perfusion Laser Doppler Image Analysis*

The LDPIWin software (Perimed, Inc., Sweden) was used to analyze the hindlimb laser Doppler images. Both feet were manually traced in each Doppler image (Figure 2.1, p. 14) and measured for mean intensity. A mean intensity ratio was calculated by dividing the mean intensity of the foot on the ligated side with that on the control side. This ratio served as a metric for the extent of perfusion or reperfusion in ligated hindlimbs.

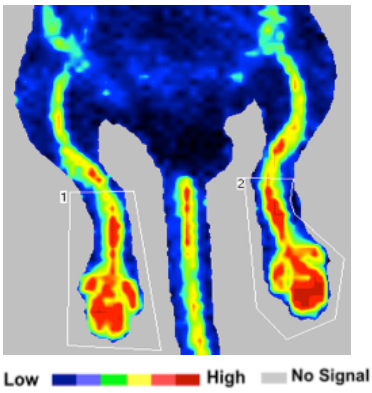

Item	Min	Max	Std.dev	Mean	Change	% Change	Median	Sites	ROI2/ROI1
ROI 1	1.13	10	2.68	5.3	ref	ref	4.89	172	1.043396
ROI 2	0.45	10	2.88	5.53	0.24	4.45	5.42	173	

Figure 2.1 Sample LDPI scan of hindlimbs and mean intensity analysis of feet. The feet are manually traced and measured for mean intensity. A perfusion ratio is calculated by dividing the mean intensity on the ligated side (#2 trace, i.e. ROI 2) by the mean intensity on the control side (#1 trace, i.e. ROI 1). This particular scan was taken before femoral artery ligation surgery.

2.2.4 *Gracilis Muscle Harvesting and Immunostaining*

The animal was first anesthetized with an I.P. injection of ketamine (0.12 mg/g mouse), xylazine (0.012 mg/g mouse) and atropine sulfate (0.00008 mg/g mouse), and then situated on a heating pad with the feet taped to the surgical stage such that the inner thighs were easily accessible. For each hindlimb, an anterior-posterior skin incision approximately 2 cm long was made along the saphenous artery. A second lateral-medial skin incision also about 2 cm long was made along the centerline of the GM, which then exposed the muscle. Warmed Ringer's solution (137.9 mM NaCl, 4.7 mM KCl, 1.2 mM $MgSO_4$, 1.9 mM $CaCl_2$, 23 mM $NaHCO_3$) containing the potent vasodilator adenosine (10^{-4} mM, Sigma, St. Louis, MO) was suffused over the muscle for 30 minutes. Afterwards, the skin was reflected back by blunt dissection to expose the entire GM and its surrounding area.

After euthanasia with an injection of pentobarbital sodium solution (0.2ml/mouse), the left ventricle of the heart was cannulated with a butterfly needle (27 GA × 0.38 ×12 IN, Saf-T E-Z Set, Becton Dickinson & Co., Sparks, MD) and the right atrium was cut to allow for removal of remaining blood with infusions of 10 ml of 2% heparinized Tris-buffered saline with $CaCl_2$, 10 ml of Tris-buffered saline with $CaCl_2$, and 10 ml of 4% paraformaldehyde (PFA)(Sigma, St. Louis, MO) at 1 ml/min with an infusion pump (Standard infusion Only PHD 22/2000 Syringe Pump, Harvard Apparatus, Holliston, MA). While the 2% heparinized Tris-buffered saline was infused, the region of the GM between the saphenous artery and the proximal feeder was carefully dissected free from the underlying muscles. After the blood removal process was completed, about 1 ml of 4% PFA was suffused over each GM and the muscles were left to fix *in situ* for approximately 30 minutes.

After fixation, the GMs were excised and treated with type I collagenase (3 mg/ml, Sigma, St. Louis, MO) in phosphate buffered saline (PBS) for 30 minutes on a rotating plate set at minimum speed to digest the type I collagen in the connective tissue between muscle fibers. Afterwards, the muscles were placed in a 1:200 Cy3-conjugated monoclonal anti-smooth muscle α-actin (clone 1A4, Sigma, St. Louis, MO) solution of 0.1% saponin and 2% bovine serum albumin (BSA) in PBS at 4°C for 3 nights. The muscles were then washed in 0.1% saponin in PBS for a total of 60 minutes (3 washes of 20 minutes each with fresh 0.1% saponin in PBS each time) and in PBS for 30 minutes on a rotating plate set at minimum speed, and then were stored in a 50/50 mixture of PBS and glycerol at -20°C.

2.2.5 GRACILIS MUSCLE IMAGING AND ANALYSIS

For imaging, the muscles were mounted on microscopic slides with PBS and temporarily sealed with glass cover slides. GMs were observed with a 4x air objective on a Nikon TE-300

inverted microscope (Nikon, Melville, NY) and images were acquired with a Microfire™ digital camera (Model S99809, Olympus America, Melville, NY) and PictureFrame software (Optronics Corp., Muskogee, OK) used in conjunction with a mercury lamp. Using the photomerge function in Photshop CS2 (Adobe Systems Inc., San Jose, CA), composite images of GMs were created from scans of individual portions.

The images of smooth muscle α-actin positive vessels within the GMs were analyzed using the ImageJ software package by measuring the anterior and posterior collateral vessel diameters at approximately 10 locations in between the muscular branch and the saphenous artery.

2.2.6 STATISTICAL ANALYSIS

For the C57BL/6 and BALB/c ligation-reperfusion profiles, data were first tested for normality and equal variance. Once both tests were passed, a t-test was performed for comparison between the two strains within the same time point. If the equal variance test failed, a Mann-Whitney Rank Sum Test was performed instead.

For the BALB/c GM collateral vessel diameter measurements, diameters from the same vessel within the same treatment group across time points were first tested for normality and equal variance, and then a One-Way Analysis of Variance (ANOVA) was performed. For comparison between the same vessel across different treatment groups within the same time point, data were first tested for normality and equal variance. Once both tests were passed, a t-test was performed. If the equal variance test failed, a Mann-Whitney Rank Sum Test was performed instead.

Statistical significance was assessed at $p<0.05$. All statistical procedures were performed using SigmaStat version 3.5 software (Systat Software Inc., San Jose, CA).

2.3 RESULTS AND DISCUSSION

From the pre-ligation and post-ligation images in Figure 2.2 (p. 18), the effect of femoral artery ligation is evident in both the C57BL/6 and BALB/c mice as feet on the ligated side all exhibit very low perfusion post-ligation. For additional evidence of ligation, microCT scans of the BALB/c mice proximal hindlimbs (Figure 2.3, p. 19) clearly show a discontinued femoral artery at the ligation site.

From the sample laser Doppler scans on days 4, 7, and 14 (Figure 2.2, p. 18), blood flow restoration to the ischemic foot over time is apparent. However, after post-ligation and onwards there is a noticeable difference in reperfusion levels between the two strains at each time point with the BALB/c mice seeming to recover at a slower rate. Quantitative analyses of those Doppler images support that observation (Figure 2.4, p. 19). Comparing the ligation-reperfusion profiles of the two mouse strains, it is evident that the window for therapeutic interventions in the BALB/c is much larger than that in the C57BL/6, making the BALB/c a more ideal candidate for ultrasound and microbubble-mediated therapeutics studies.

Additionally, Figures 2.5 (p. 20) and 2.6 (p. 21) clearly show significant remodeling of the collateral vessels in the gracilis muscles of BALB/c mice post femoral artery ligation, which confirms the muscle as a good experimental target for use in future vascular remodeling studies where perturbations may be introduced to study the efficacy of treatment modalities or associated remodeling mechanisms. The BALB/c gracilis muscle was therefore chosen for the studies on how various ultrasound peak negative pressures affect the distribution of nanoparticle delivery (Chapter 5) and inflammatory response (Chapter 6) caused by ultrasound-microbubble interactions.

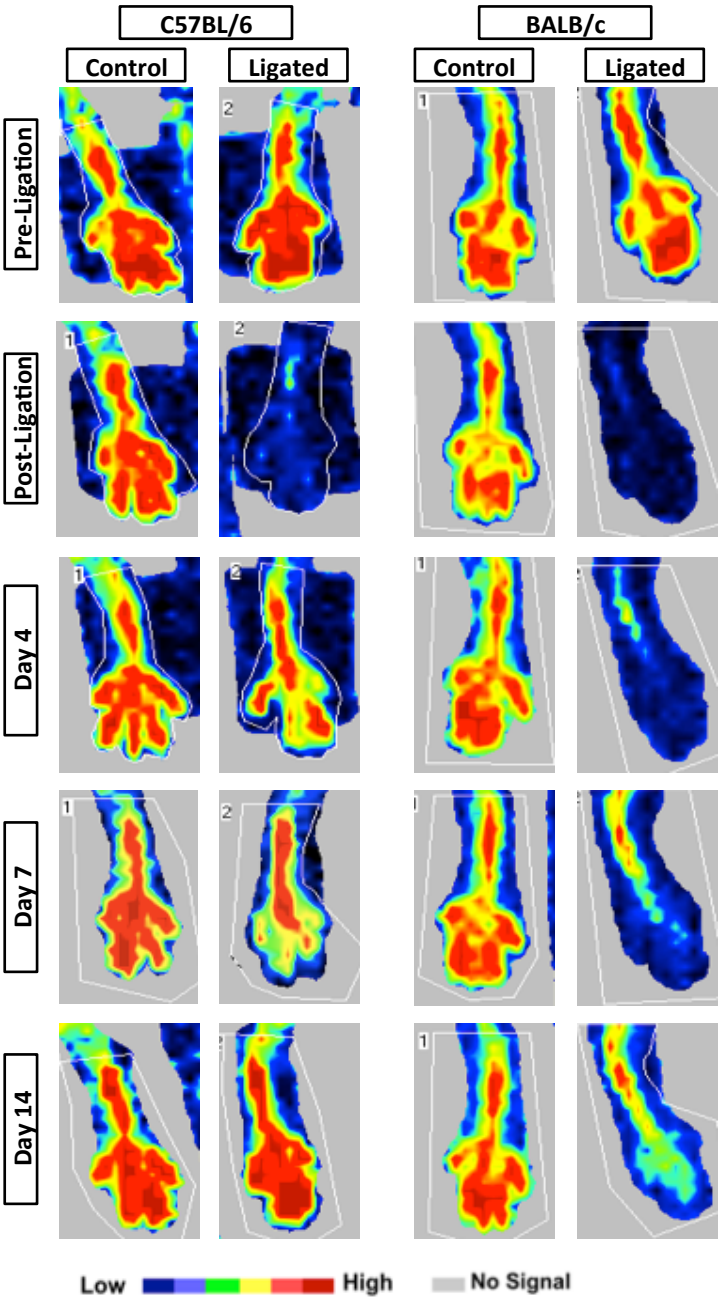

Figure 2.2 Sample LDPI scans pre-ligation, post-ligation, and on days 4, 7 and 14 of C57BL/6 and BALB/c mice feet. The white lines are manual traces made during intensity measurements.

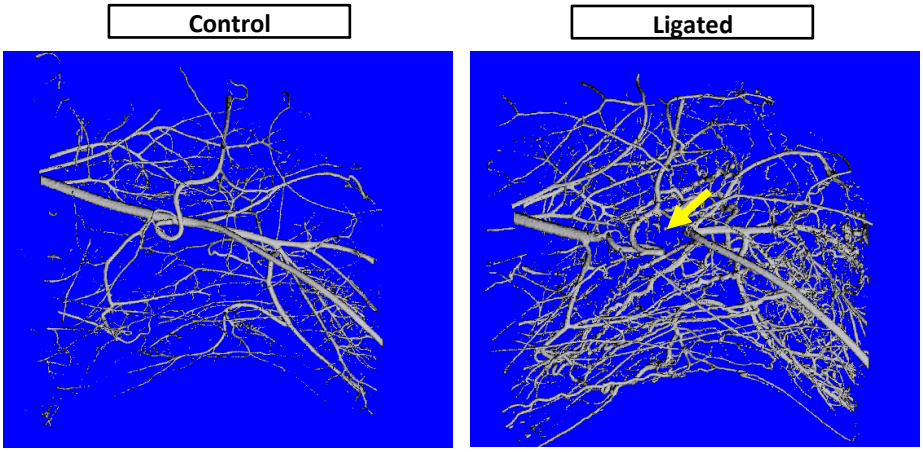

Figure 2.3 Sample microCT images of the proximal hindlimbs of BALB/c mice from control (left) and femoral artery-ligated (right) groups. The ligated side was scanned 14 days after femoral artery ligation. The ligation site is denoted with a yellow arrow. See Appendix B for the microfil injection procedure performed in preparation for microCT scans.

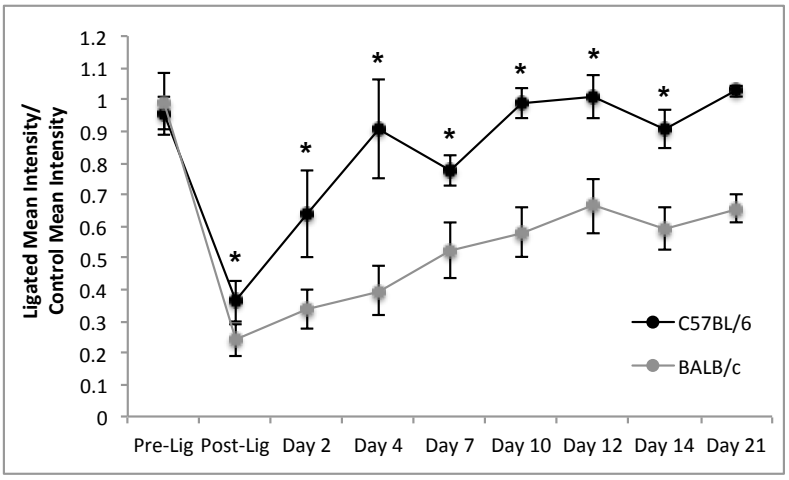

Figure 2.4 Ligation-reperfusion profiles for C57BL/6 and BALB/c mice. *Indicates significantly different than BALB/c within the same time point; Post-Lig at P =< 0.001, Day 2 at P = 0.002, Day 4 at P = 0.002, Day 7 at P = 0.004, Day 10 at P <= 0.001, Day 12 at P <= 0.001, and Day 14 at P <= 0.001.

Table 2.1 Specific number of mice for each strain at each time point in which LDPI data was collected from.

	Pre-Lig	Post-Lig	Day 2	Day 4	Day 7	Day 10	Day 12	Day 14	Day 21
n (C57BL/6)	6	8	8	4	2	4	6	7	2
n (BALB/c)	34	34	4	19	9	4	4	12	2

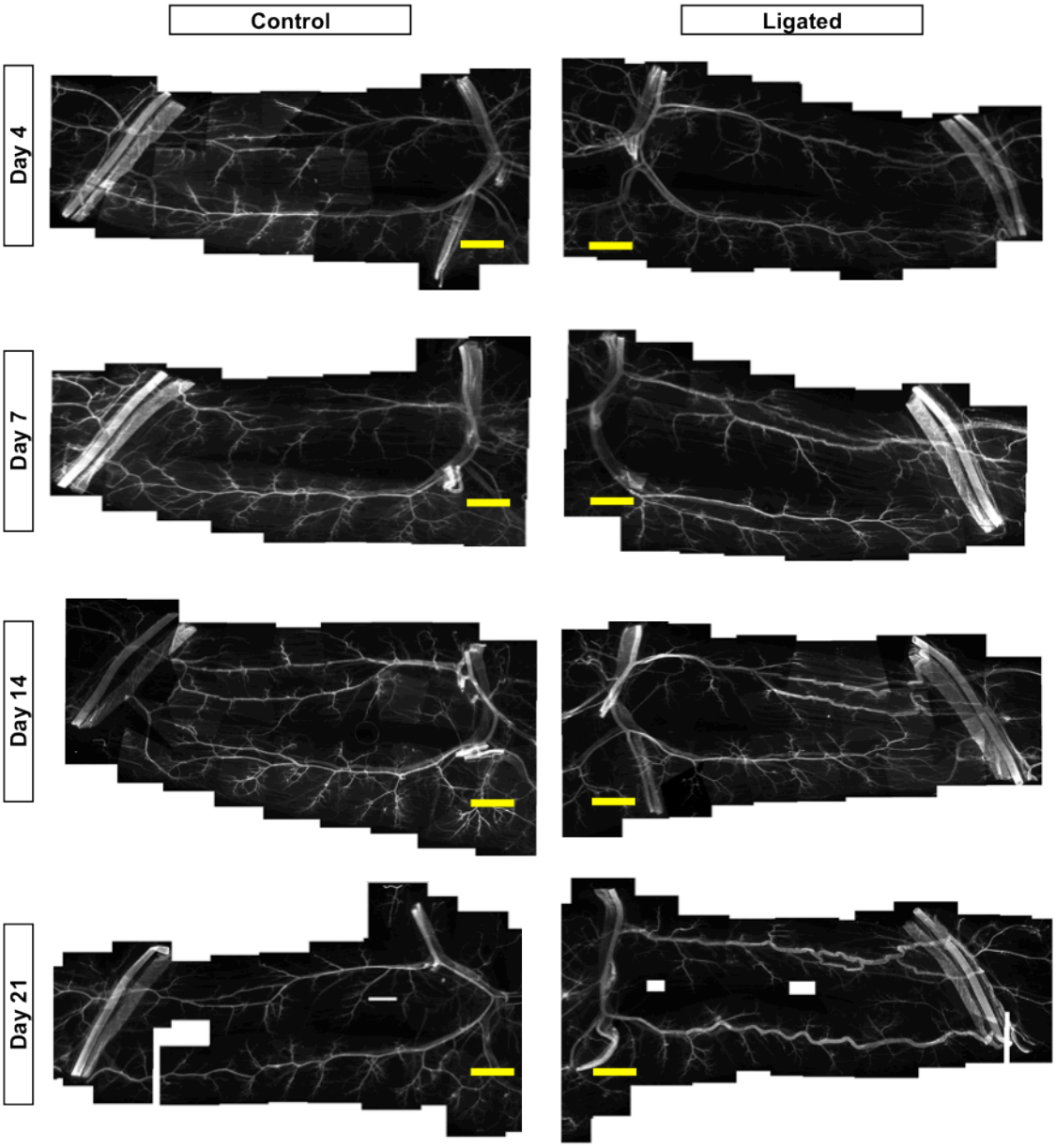

Figure 2.5 Representative images of smooth muscle α-actin positive vessels in gracilis muscles from BALB/c mice. Scale bar = 1 mm.

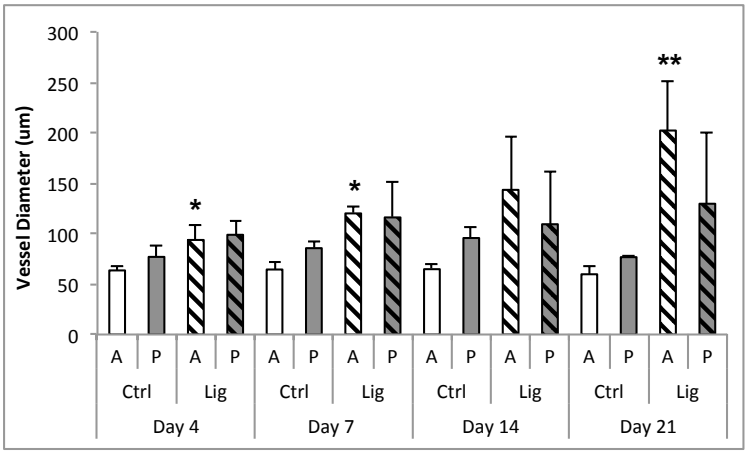

Figure 2.6 Gracilis muscle anterior (A) and posterior (P) collateral vessel diameter measurements from the control (Ctrl) and ligated (Lig) groups on days 4, 7, 14 , and 21 post femoral artery ligation.
*Indicates significantly different than the same collateral vessel on the control side within the same time point; Day 4 at P = 0.003, Day 7 at P =< 0.001.
**Indicates significantly different than the same collateral vessel within the same treatment group on day 4.

Table 2.2 Specific number of BALB/c mice for each time point in which collateral vessel diameter measurements were made.

	Day 4	Day 7	Day 14	Day 21
n (BALB/c)	5	3	3	2

CHAPTER 3: DEVELOPMENT OF AN ULTRASOUND-MEDIATED MICROBUBBLE DESTRUCTION PROTOCOL IN THE ISCHEMIC MOUSE HINDLIMB

3.1 INTRODUCTION

Past ultrasound-microbubble (US-MB) studies from our group using the mouse hindlimb were done with the skin above the gracilis muscle reflected (Chappell, Song, Burke, Klibanov, & Price, 2008a; Chappell, Song, Klibanov, & Price, 2008b) to prevent acoustic attenuation by MBs in the superficial tissue (Nyborg, 2007; Song et al., 2008). Due to the invasiveness of the procedure, inflicted risk of infection from the large incision wound, and impracticality of removing superficial tissue every time for treatment, it was necessary to develop a protocol for attaining US-MB-induced bioeffects in deeper tissue without temporary skin removal. To this end, a working protocol for acquiring petechiae in the gracilis muscles of BALB/c mice with overlaying skin intact was derived through a trial and error process of adjusting the US pulsing and MB infusion parameters. It is known that the extent of creation of such bioeffects depend on factors such as US power (Miller & Quddus, 2000), pulsing interval (Song et al., 2002), and MB concentration in tissue (Miller & Quddus, 2000; Song et al., 2008). While petechiae are not necessarily required as a sign of acoustic attenuation in the superficial tissue being overcome, the presence or lack of petechiae served as a convenient and obvious indicator. Also, the particular US pulsing protocol associated with sufficient petechiae observed would then potentially serve as a reference for adjusting to weaker pulsing parameters.

To minimize the effect of MB-induced acoustic attenuation, MB concentration in tissue at any time was lowered by infusing the desired amount of MBs into the mouse over a longer period of time, and hence at a lower rate. The composition of a pulse was changed by increasing the number of bursts within a pulse and by increasing the number of sinusoids within a burst (Figure 3.1, p. 28). The rationale behind this modification was that the longer bursts and longer

pulses would be capable of clearing the attenuating MBs in the superficial layer and still reach deeper tissue. Also, studies have demonstrated positive correlation between pulse length and extent of cavitation damage (Chen, Brayman, Matula, Crum, & Miller, 2003; Tu et al., 2006)

After numerous attempts using various pulsing parameter combinations and MB infusion durations, petechiae were finally first observed in the gracilis muscle (Figure 3.2, 5000 waves × UTMD, p. 29) by applying 5000 consecutive 1-MHz sinusoids of 1 volt peak-to-peak amplitude in one burst, 10 bursts each spaced 100 msec apart to form one pulse, and 72 pulses with 10 sec intervals in between each pulse to form one complete treatment of 12 minutes (Figure 3.1B, p. 28). However, since the petechiae were considerably massive and there was likely more damage in the muscle than treatment potential, it became necessary to adjust the protocol further to yield smaller total areas of hemorrhaging. In particular, lower sinusoid numbers of 2500, 500, and 300 were tested as an alternative to the 5000.

3.2 EXPERIMENTAL METHODS

For these experiments, 6 BALB/c mice (25 grams, 9 – 11 weeks old, Harlan Laboratories, Inc., Dublin, VA) were tested, with 2 mice per sinusoid number. The experimental time course for each mouse was femoral ligation on day 0 and USMB application on day 4.

3.2.1 FEMORAL ARTERY LIGATION

Animals were anesthetized by an I.P. injection of ketamine (0.12 mg/g mouse), xylazine (0.012 mg/g mouse), and atropine sulfate (0.00008 mg/g mouse). Once the mice were under anesthesia, the eyes were covered with an ophthalmic ointment (Duratears, Alcon Laboratories, Inc., Forth Worth, TX) to prevent against light damage and dehydration. The inner thigh of each leg and the surrounding region were depilated and cleaned with a Betadine (Purdue Frederick Company, Norwalk, CT) wipe followed by an ethanol swab. The Betadine-ethanol cleaning

sequence was then repeated 2 more times with short breaks of approximately 20 seconds in between to prevent the animal from becoming hypothermic.

All surgical instruments were sterilized with high-pressure saturated steam at 121°C in an autoclave for around 35 minutes and allowed to cool before surgery. After the depilated area on the animal was cleaned, the animal was placed supine on a warmed surgical stage. A sterile drape covered the animal almost entirely, the inner thighs were exposed through openings in the drape and the nose and mouth were exposed at the edge of the drape. Viewing through a Zeiss surgical dissecting microscope (Stemi 2000, Carl Zeiss, Inc., Thornwood, NY), on one leg a skin incision less than 5 mm long was made directly along the femoral artery immediately distal to where the epigastric artery branches off. The fascia and fat between the skin and underlying muscle were gently cleared by blunt dissection to expose the artery-vein pair running distal to where the epigastric artery-vein pair branches off of the femoral artery-vein. A separation of less than 4 mm in length was made between the artery and vein, sufficient for ligature placement. Special care was taken to leave the nerve running along this vessel pair intact and minimally disturbed. Two sterile pieces of silk sutures (6-0, Deknatel, Inc., Fall River, MA) were then tied at less than 2 mm apart around the separated section of the artery. The artery segment between the two ligatures was then severed with micro dissecting scissors. The skin incision was closed with sutures (5-0 Proline, Ethicon, Somerville, NJ) and the animal was left to recover on a heating pad. As the anesthesia wore off, an I.P. injection of buprenorphine (0.03 ml/animal, Reckitt Benckiser Pharmaceuticals Inc., Richmond, VA) was given, followed by a second dose 8-12 hours later.

3.2.2 JUGULAR VEIN CANNULATION

Animals were anesthetized with an I.P injection of ketamine (0.12 mg/g mouse), xylazine (0.012 mg/g mouse) and atropine sulfate (0.00008 mg/g mouse). The neck and inner thigh of each leg were depilated. After being secured on a warmed surgical stage, a skin incision was made along the right jugular vein. The jugular vein was exposed by blunt dissection and carefully separated from the surrounding connective tissue. Two pieces of 6-0 black braided silk sutures (Ethicon, Somerville, NJ) were placed under the jugular vein to provide tension as a PE-10 tubing (Inner diameter: 0.28 mm, Outer Diameter: 0.61 mm, Becton Dickinson & Co., Sparks, MD) attached to a 3-way stop cock and then a syringe of 1% heparin saline (0.9%) was inserted through a small incision into the jugular vein and tied in place with the sutures.

Although more invasive, time-consuming, and can only be done to the animal once, a jugular vein cannulation was chosen over a tail vein cannulation due to its more secured nature. The tail veins are located on the two sides of the tail, which with the mouse required in a supine position for US-MB treatment, are considerably difficult to cannulate. The inserted cannula in a tail vein is also challenging to keep in place during treatment as any slight movement could potentially remove the cannula or even cause the cannulating needle to pierce through the cannulated vein.

3.2.3 ULTRASOUND-MICROBUBBLE TREATMENT

After the jugular vein was cannulated, the feet were gently taped to the surgical stage such that the inner thighs were easily accessible. A 1-MHz unfocused transducer (A303S, Olympus NDT Inc., Waltham, MA) with a 0.5-inch (1.27 cm) diameter was manually positioned over the hindlimb with a layer of air bubble-free ultrasound transmission gel (Aquasonic® 100 ultrasound transmission gel, Parker Laboratories, Inc., Fairfield, NJ) between it and the skin

surface. Albumin microbubbles (approximately 1×10^9 MB/ml stock concentration, mean diameter of approximately 2 μm) generously provided by Dr. Alexander Klibanov from the Cardiovascular Medicine Department at the University of Virginia were serially diluted to approximately 1.56×10^7 MB/ml in 0.9% saline solution with a 1 ml syringe (1 ml Sub-Q 26G⅝, Becton Dickinson & Co., Franklin Lakes, NJ). Special care was taken to draw MBs into the syringe slowly to lessen MB shearing and to replace the MB stock vial headspace with high-molecular-weight perfluoropropane gas to minimize stock MB destabilization. Additionally, extra attention was also put on promoting homogenous MB size distribution throughout the syringe by gently rolling and rocking the syringe about its cylindrical and medial axis as larger bubbles might have floated more to lumen edges during the drawing process. The syringe was then connected to the 3-way stopcock and MBs were infused at a rate of 13.333 μl/min with an infusion pump (Standard infusion Only PHD 22/2000 Syringe Pump, Harvard Apparatus, Holliston, MA). Approximately 0.14 ml dead space of 1% heparin saline (0.9%) originally in the stop cock and jugular vein catheter tubing was replaced in the first 11 min 35 seconds of infusion with MBs being infused into the mouse immediately after. 11 min and 45 seconds into the infusion process, US pulsing was triggered with a LabView software program (National Instruments, Austin, TX) for 12 minutes. Each pulse consisted of 10 bursts each spaced 100 msec apart, each burst, depending on the treatment group, consisted of 5000, 2500, 500, or 300 consecutive 1-MHz sinusoids of 1 volt peak-to-peak amplitude from a waveform generator (Tektronix AFG-310, Sony Tektronix, Beaverton, OR). The waveform signal was amplified by a 55-dB RF power amplifier (model 3100LA, ENI, Inc.) and fed into the transducer. In between pulses, a 10-second interval allowed for MB reperfusion into the targeted region. A needle hydrophone (model PVDF-Z44-0400, Specialty Engineering Associates, Sunnyvale, CA) later

measured the system's peak negative pressure to be at approximately 0.8 to 0.9 MPa at roughly where the gracilis muscle lies. During treatment, 0.16 ml of the diluted MB solution was infused into the mouse. In total, 0.3 ml of solution was introduced into the mouse intravenously in about 23 minutes, which is well under the recommended maximum of 0.625 ml delivered to a mouse of 25 grams via slow intravenous infusion according to Fox et al., 2009 and Patricia Foley, DVM, the Director of the Office of Animal Welfare at the University of Virginia (personal communication, November 18, 2008).

3.2.4 Hindlimb Imaging for Petechiae

After USMB treatment, for each hindlimb an anterior-posterior skin incision approximately 2 cm long was made along the saphenous artery. A second lateral-medial skin incision also about 2 cm long was made along the centerline of the GM. The skin was then reflected back by blunt dissection to expose the entire GM. Both hindlimbs were observed using a macroscope at 5x and 8x and images were taken with a Microfire™ digital camera (Model S99809, Olympus America, Melville, NY) and PictureFrame software (Optronics Corp., Muskogee, OK).

3.3 Results and Discussion

As the number of sinusoids within a burst was decreased from 5000 to 2500 to 500 to 300, it was apparent that the extent of hemorrhages in the deeper tissues diminished accordingly (Figure 3.2, p. 29). The extent of petechiae observed at the 300-sinusoid level was similar to that seen in past USMB therapeutic studies when the skin over the gracilis muscle was reflected back (Chappell, Klibanov, & Price, 2005), and was deemed likely appropriate for the purposes of this project. Therefore a sinusoid number of 300 was used for all the remaining studies with USMBs.

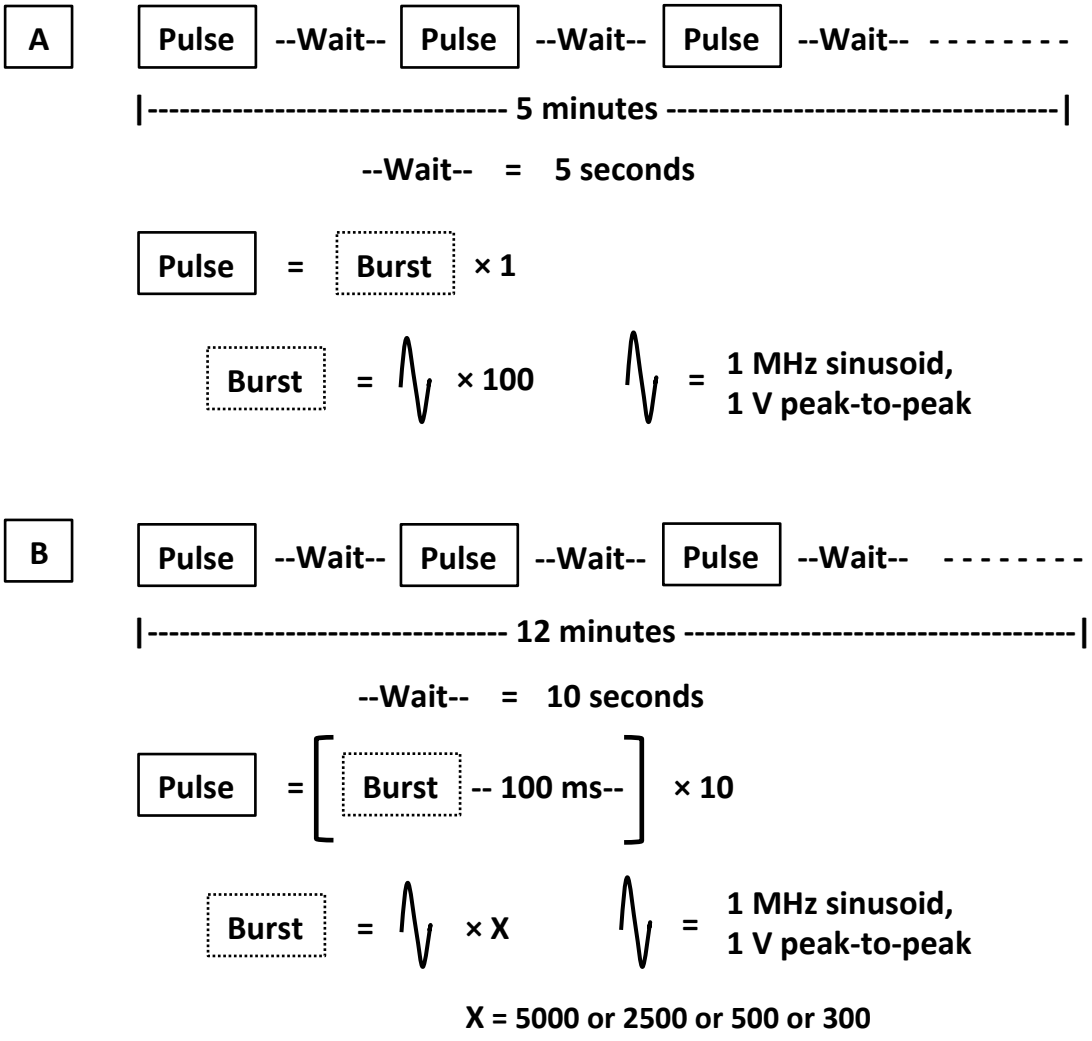

Figure 3.1 Ultrasound pulsing protocols for USMB application on the proximal hindlimb when the skin above the gracilis muscle was (A) removed and (B) intact.

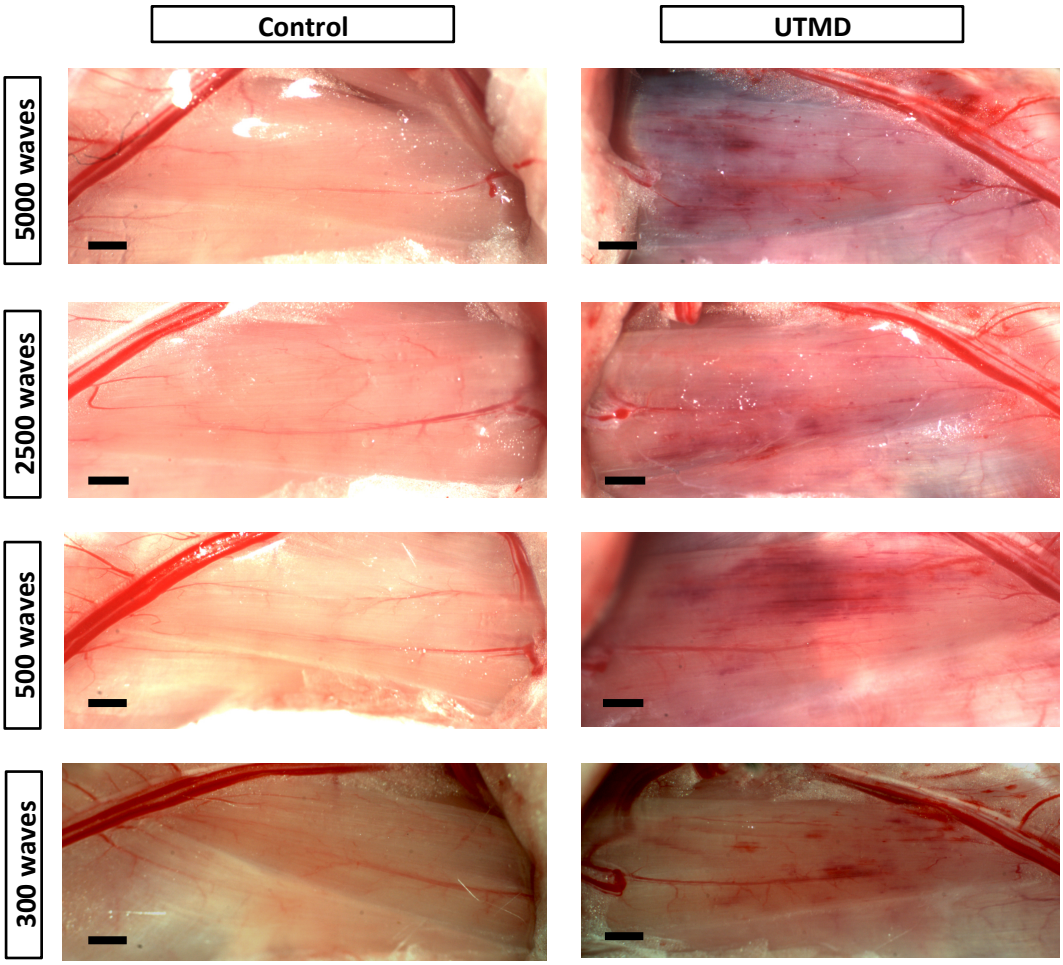

Figure 3.2 Sample images of the gracilis muscle region post UTMD application with skin intact. Scale bar = 1 mm.

CHAPTER 4: CHARACTERIZATIONS OF THE ULTRASOUND AND MICROBUBBLE DELIVERY SYSTEMS

4.1 INTRODUCTION

In preparation for testing the effects of various ultrasound (US) peak negative pressure (PNP) levels on the extent of nanoparticle (NP) delivery (Chapter 5) and inflammatory response (Chapter 6) in the ischemic mouse skeletal muscle, the specific voltage inputs that would yield the desired pressures had to be acquired. Therefore, the 1-MHz unfocused transducer (A303S, Olympus NDT Inc., Waltham, MA) used was characterized at various voltage inputs ranging from 0.05 V to 1 V at distances 3 mm to 10 mm directly away from the transducer face to generate corresponding peak negative pressure profiles. The various distances were associated with the specific thickness of ultrasound gel to place between the transducer and the skin surface in order to apply the desired PNP.

Previously during the trial and error process of getting petechiae to occur in deeper tissue (detailed in Chapter 3), a growing accumulation of microbubbles over time was observed at the top edge of the syringe lumen. Instead of being carried from the syringe into the catheter as originally assumed, the accumulated MBs appeared to remain "stuck" in the syringe throughout the entire MB infusion process. It was suspected that the slow infusion rate of 13.333 μl/min was too low to overcome the natural buoyancy of MBs - especially those of larger diameters (Feshitan, Chen, Kwan, & Borden, 2009) - in the syringe, which in turn would likely have caused an unanticipated total number decrease and size distribution shift of MBs outputted from the infusion system and delivered into the mouse. Also, albeit at a slow infusion rate, since the MBs were infused through a rather large gauged (specifically 30G) needle, it is possible that the small needle inner diameter could have created a large pressure differential that collapse bubbles and thus altered the intended MB concentration and size distribution to be delivered as well

(Browning et al., 2011; Talu, Powell, Longo, & Dayton, 2008). Due to the fact that MB concentration affects the extent of US-induced cavitation (Tu et al., 2006) and acoustic attenuation (Song et al., 2008), while MB diameter affects potential MB biodistribution (Sirsi, Feshitan, Kwan, Homma, & Borden, 2010), echogenicity and resonant frequency (de Jong, Bouakaz, & Frinking, 2002; Morgan et al., 2000), it was critical to know more accurately the MB population that was being introduced into mice. To this end, microbubble populations outputted from the microbubble delivery system (i.e. syringe to needle to catheter) were characterized using a Multisizer™ 3 Coulter Counter ® (Beckman Coulter, Brea, CA) and attempts were made to minimize the loss of bubbles through the infusion process by increasing the infusion rate by 5x and stirring the bubbles within the syringe with the anticipation of possibly overcoming the effect of bubble flotation.

4.2 Experimental Methods

4.2.1 Ultrasound Transducer Characterization

Transducer characterization was performed with the generous help of Dr. Linsey Phillips from the Hossack Lab and all equipment used were provided by the Hossack Lab as well.

Briefly, for each voltage input the transducer was first aligned in a degassed water bath 10 mm away from the hydrophone on an air table. Using a LabVIEW program-controlled motion stage, the hydrophone was moved directly towards the transducer in 0.2 mm increments until it was at 3 mm away from the transducer. At each distance, the transducer emitted 5-cycle pulses at a pulse repetition frequency of 100 Hz as a LabVIEW program (provided by the Hossack Lab) averaged the voltage measurements of 200 pulses collected by the hydrophone. This process was repeated for voltage inputs ranging from 0.05 V to 1 V. The data acquired through LabVIEW was then analyzed in MATLAB to yield the PNPs corresponding to each of

the voltage inputs for each of the distances directly away from the transducer (Figures 4.1, p. 34; Figure 4.2, p. 35).

4.2.2 MICROBUBBLE DELIVERY SYSTEM CHARACTERIZATION

Albumin microbubbles (approximately 3.54×10^8 MB/ml stock concentration, mean diameter of 3.53 μm) generously provided by Dr. Alexander Klibanov from the Cardiovascular Medicine Department at the University of Virginia were diluted to approximately 3.54×10^7 MB/ml in 0.9% saline solution with a 1 ml syringe (1 ml Sub-Q 26G⅝, Becton Dickinson & Co., Franklin Lakes, NJ). Special care was taken to slowly draw MBs into the syringe to lessen MB shearing and to replace the MB stock vial head space with high-molecular-weight perfluoropropane gas to minimize stock MB destabilization. Additionally, extra attention was also put on promoting homogenous MB size distribution throughout the syringe by gently rolling and rocking the syringe about its cylindrical and medial axis as larger bubbles might have floated more to lumen edges during the drawing process. The syringe was then attached to the cannula made of a 20 cm PE-10 tubing (Inner diameter: 0.28 mm, Outer Diameter: 0.61 mm, Becton Dickinson & Co., Sparks, MD) pre-connected to a 30G needle (30G1/2, Precison Gluide, Becton Dickinson & Co., Franklin Lakes, NJ) carefully to avoid air bubbles. MBs were infused at rates of 13.333 μl/min or 66.666 μl/min using an infusion pump (Standard infusion Only PHD 22/2000 Syringe Pump, Harvard Apparatus, Holliston, MA) after 0.04 ml of dead space of 1% heparin saline (0.9%) originally in the cannula was cleared with a manual infusion at a rate of around 1 ml/min. For MBs that were stirred during infusion, a 2 mm diameter × 7 mm long micro stir bar (Fisher Scientific, Pittsburgh, PA) was inserted into the 1 ml syringe prior to MB dilution, and during infusion a mini magnetic stirrer (Fisher Scientific, Pittsburgh, PA) was manually hovered over and along (back and forth) the syringe to drive stirring.

To get measurements of the MB populations delivered into the mouse, the infused MBs were sampled at approximately 3 minutes after infusion began for 13.333 μl/min and 66.666 μl/min infusions and again at around 10 minutes for 13.333 μl/min infusions. The MB samples were then quantified using a Multisizer™ 3 Coulter Counter ® (Beckman Coulter, Brea, CA) provided by the Klibanov Lab.

4.3 RESULTS AND DISCUSSION

4.3.1 ULTRASOUND TRANSDUCER CHARACTERIZATION

The A303S 1-MHz unfocused transducer was characterized by acquiring the PNP profiles at voltage inputs ranging from 0.05 V to 1 V at distances 3 mm to 10 mm away from the transducer. Figure 4.1 (p. 34) shows a few sample profiles of PNP with respect to distance at voltage inputs of 0.1 V, 0.2 V, 0.3 V and 0.8 V. From Figure 4.1, it appears that PNP changes quite readily over distances up to about 6 to 7 mm from the hydrophone, therefore to have better control over the PNP applied to the target tissue, the transducer face should be kept at least 7 mm from the target tissue. With a minimal distance of 7 mm in mind, Figure 4.2 (p. xx) shows a few sample profiles of PNP with respect to voltage input at distances of 7 mm, 8 mm, 9 mm, and 10 mm away from the transducer where at 10 mm, the same voltage inputs seemed to yield the largest range of PNPs with maximum PNP of 0.7 MPa possible. For testing the effect of various PNP levels (specifically 0.7 MPa, 0.55 MPa, 0.4 MPa, and 0.2 MPa by inputting 0.8 V, 0.3 V, 0.2 V, and 0.1 V respectively) on nanoparticle delivery (Chapter 5) and inflammatory response (Chapter 6), a distance of 10 mm was therefore kept between the transducer face and the gracilis muscle. This was done by maintaining an approximately 8 mm layer of ultrasound gel between the transducer and the skin surface while estimating a 2 mm distance between the skin surface

and the center of the gracilis muscle (see *5.2.4 Ultrasound-Microbubble-Mediated Nanoparticle Delivery* and *6.2.3. Ultrasound-Microbubble Application*).

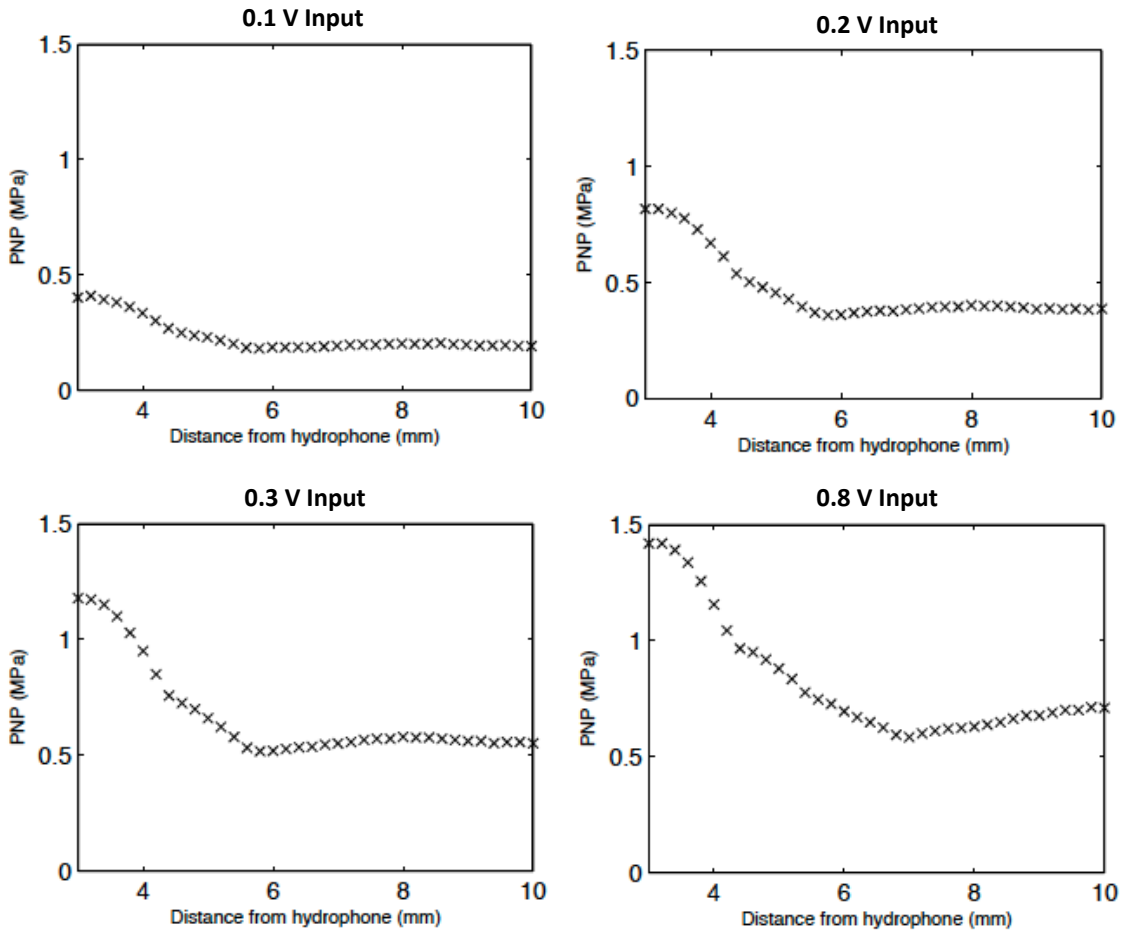

Figure 4.1 Sample peak negative pressure measurements of the unfocused A303S transducer 3 mm to 10 mm (at 0.2 mm increments) directly away from the hydrophone with fixed voltage inputs.

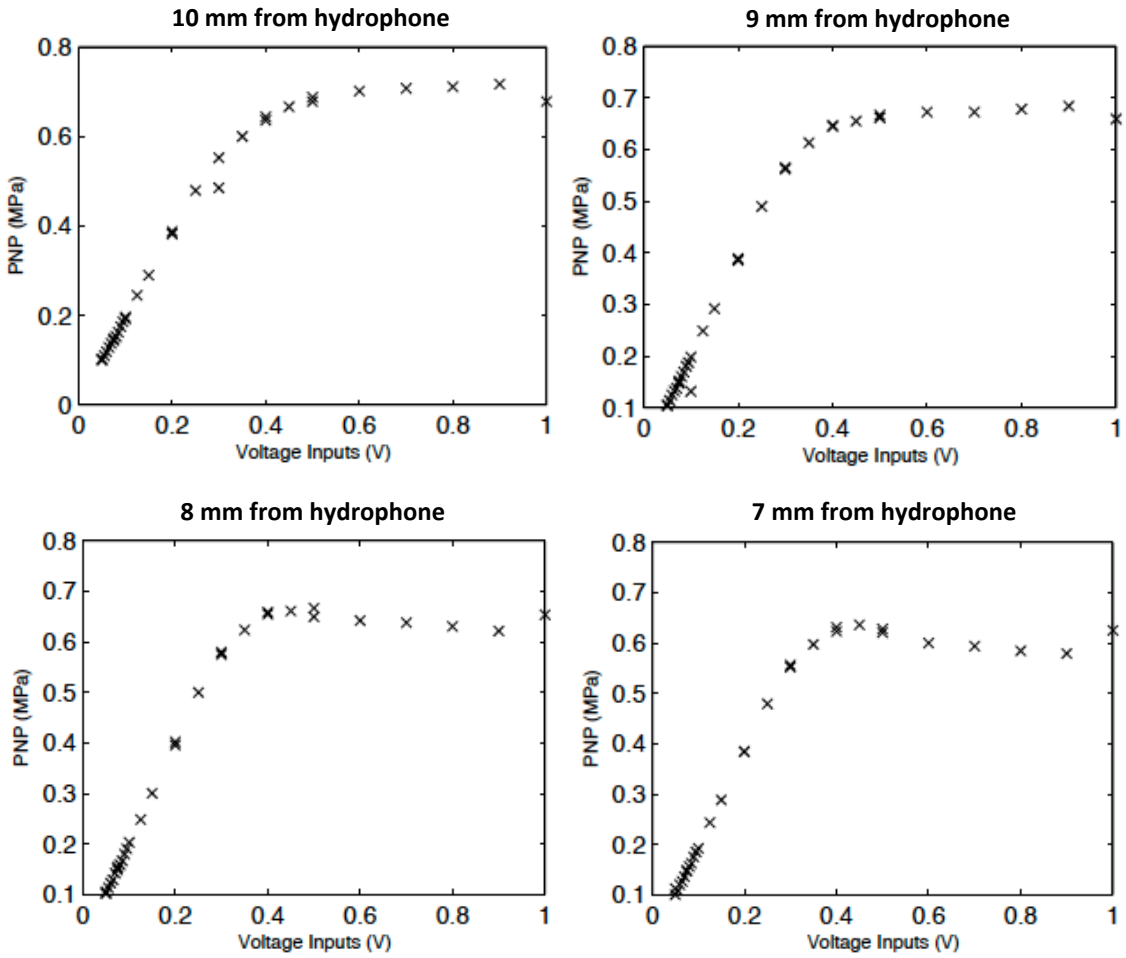

Figure 4.2 Sample peak negative pressure measurements of the unfocused A303S transducer with varying voltage inputs at fixed distances directly away from the hydrophone.

4.3.2 Microbubble Delivery System Characterization

To get the actual MB concentration and size distribution delivered into the mouse, MBs outputted from the infusion system were quantified. Figure 4.3 (p. 37) gives two representative examples. The expected distributions shown were calculated from MB distributions of stock samples in which delivered MBs were diluted from. Post infusion, there appears to be about a 60% decrease in MB concentration and 40% decrease in diameter, near complete loss of bubbles with diameters above 4 μm, and a near 50% loss of MBs in the 2 to 3 μm range, which indicates that the MBs delivered into mice via continuous infusion are actually much smaller and fewer

than assumed. Reasons for this loss has yet to be confirmed, but bubble flotation in the syringe is likely the main cause, especially under the slow infusion rate of 13.333 μl/min.

Attempts to possibly minimize bubble loss to flotation during the infusion process included increasing the infusion rate by 5x and/or magnetically stirring the bubbles while they were in the syringe (Figure 4.4, p. 38). Based on Figure 4.4B and D, it seems that increasing the infusion rate by 5x could potentially help preserve bubbles in the 2 to 4 μm diameter range. The effect of stirring, however, is rather inconclusive. When the infusion rate was at 13.33 μl/min, stirring appeared to inflict greater MB loss (Figure 4.4C), while infusion at 66.66 μl/min stirring seemed to help alleviate MB loss (Figure 4.4E). Possible explanations for this could be the nature of the stirring itself. Close observation of the mini stir bar at work revealed that instead of "stirring" in the expected manner, the 1 ml syringe provides only limited space such that the stir bar actually "wiggles" at high speed in the syringe instead. Therefore, for the 13.33 μl/min infusion rate it might have been possible that there was a greater probability of the stir bar destroying bubbles in its wiggling path within the confined syringe lumen than for the slightly higher infusion rate of 66.66 μl/min.

Overall, the suspected deviation in MB population delivered from that originally assumed was confirmed (Figure 4.3). Therefore, for MB deliveries done later in studying the effect of various PNP levels on USMB-mediated nanoparticle delivery (Chapter 5) and inflammatory response (Chapter 6), the MB populations outputted by the delivery system were quantified every time beforehand to ensure consistency across study groups. Furthermore, although the methods for minimizing the loss of bubbles with larger diameters during the infusion process were not applied in studies detailed in this thesis, for future work they may lend insight into ensuring the delivery of large monodispersed microbubbles.

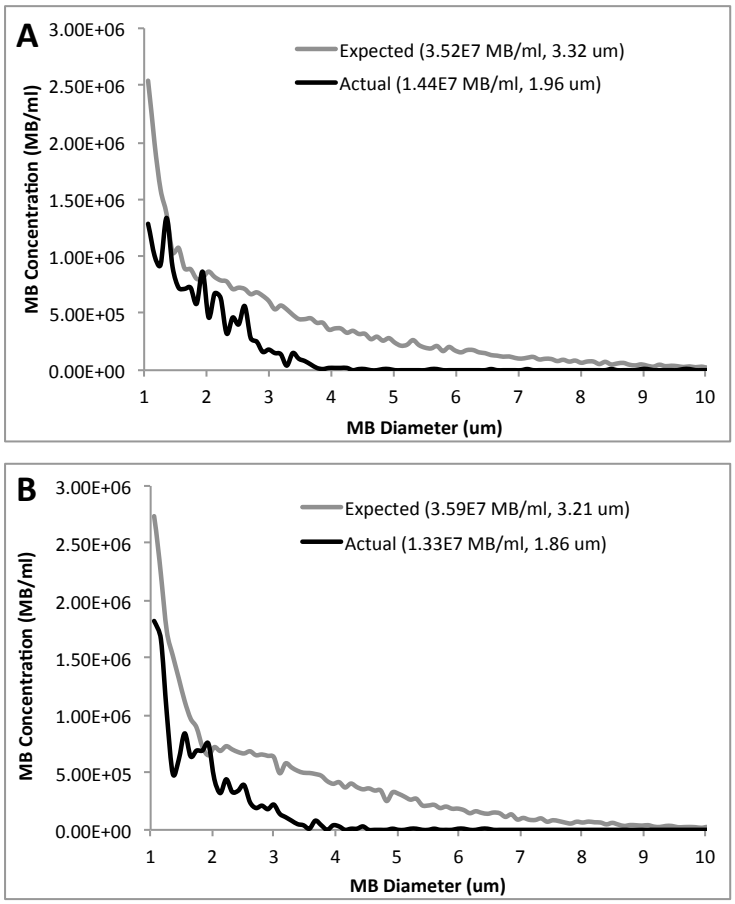

Figure 4.3 Coulter Counter ® measurements of microbubble populations post 13.33 µl/min infusion compared to that expected based on stock measurements. (A) and (B) represent results sampled from two different MB stock vials from two different manufacturing batches. Values in parentheses represent "average microbubble concentration, average microbubble diameter."

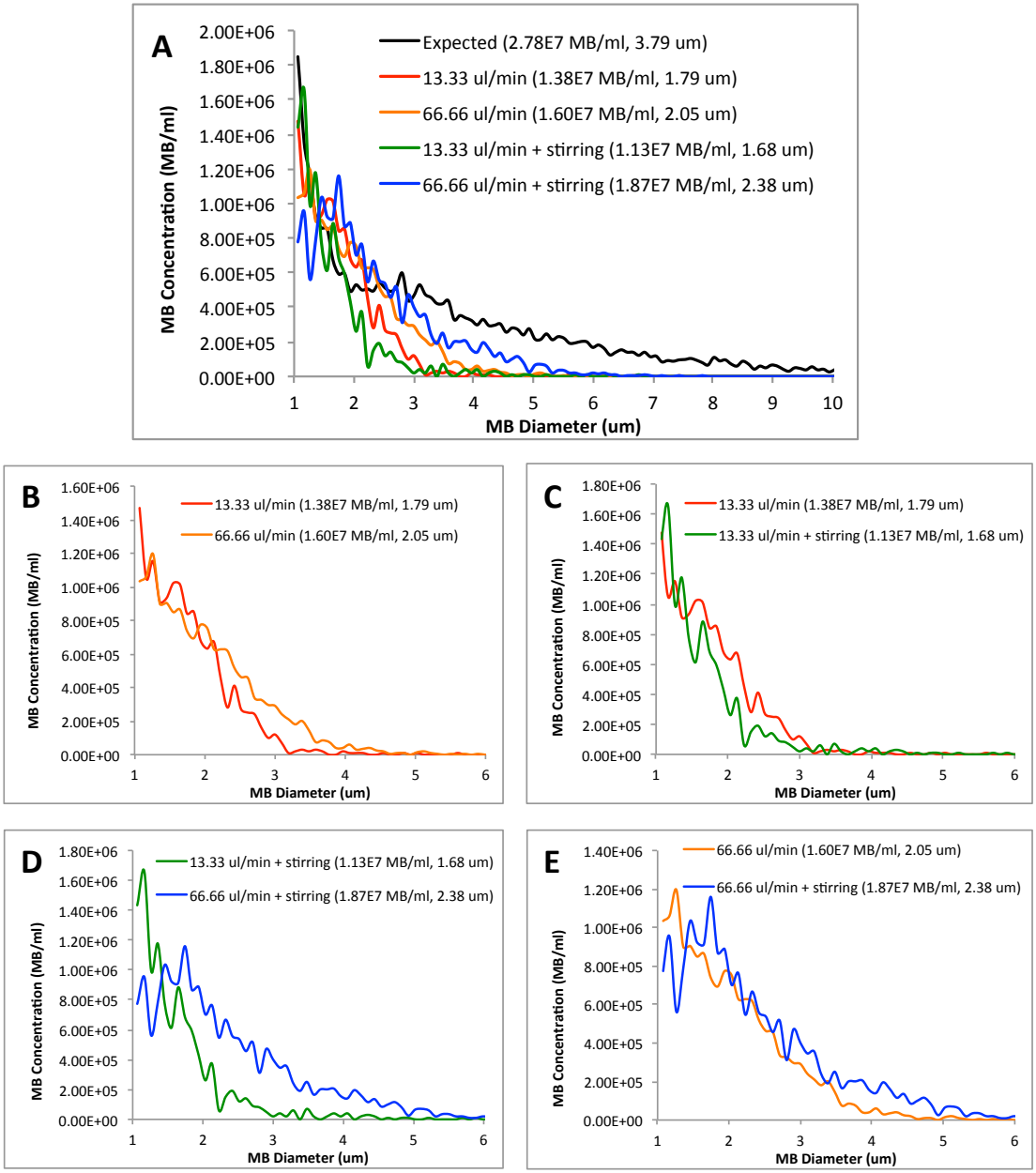

Figure 4.4 Coulter Counter ® measurements of microbubble populations post infusion. (A) Populations post infusion at 13.33 µl/min, 66.66 µl/min and infusion at those respective rates plus stirring compared to that expected based on stock measurements. (B) Populations post infusion at 13.33 µl/min compared to 66.66 µl/min. (C) Populations post infusion at 13.33 µl/min compared to 13.33 µl/min plus stirring. (D) Populations post infusion at 13.33 µl/min plus stirring compared to 66.66 µl/min plus stirring. (E) Populations post infusion at 66.66 µl/min compared to 66.66 µl/min plus stirring. Values in parentheses represent "average microbubble concentration, average microbubble diameter."

CHAPTER 5: NANOPARTICLE DELIVERY MEDIATED BY ULTRASOUND AND MICROBUBBLES

5.1 INTRODUCTION

To determine how various ultrasound (US) peak negative pressures (PNPs) affect the distribution of nanoparticles (NPs) delivered by US-MB interactions in ischemic mouse skeletal muscle, PNP levels were applied at 0.7 MPa, 0.55 MPa, 0.4 MPa, and 0.2 MPa. 50 nm red and 100 nm green fluorescent polystyrene spheres were delivered through a femoral artery or jugular vein cannula. The femoral artery route allowed the MBs to bypass filtering by the lungs where capillaries are narrowest in the body (Calliada, Campani, Bottinelli, Bozzini, & Sommaruga, 1998), as the bubbles were introduced into the hindlimb directly upstream of the US-exposed gracilis muscle. The jugular vein route delivery of MBs incorporated the effects of filtering by the lungs and longer circulation on MB populations that reach the gracilis muscle.

5.2 EXPERIMENTAL METHODS

31 BALB/c mice (25 grams, Harlan Laboratories, Inc., Dublin, VA) were used for these NP delivery studies. 16 received MB and NP delivery through jugular vein cannulations, while 15 received MBs and NPs through femoral artery cannulations. The number of mice experimented per treatment group of a different PNP applied are detailed in Table 5.1 (p. 39).

Table 5.1 Nanoparticle Delivery Study Treatment Groups

Cannulation Route	Jugular Vein				Femoral Artery			
PNP(MPa)	0.7	0.55	0.4	0.2	0.7	0.55	0.4	0.2
Number of mice	4	4	4	4	3	4	4	4

For these nanoparticle delivery studies, the experiment time course was femoral artery ligation on day 0, USMB-NP treatment on day 4, image for petechiae, and harvest USMB-NP-treated gracilis muscle (GM) immediately after. The GM whole mount was then later imaged (for femoral artery cannulation route treatment groups only), cryosectioned and stained for

endothelial cells. The resulting GM cross sections are then imaged and analyzed for NP delivery.

5.2.1 Femoral Artery Ligation

Mice received unilateral arterial occlusions and were maintained under sterile conditions throughout experimentation. Animals were anesthetized by an I.P. injection of ketamine (0.12 mg/g mouse), xylazine (0.012 mg/g mouse), and atropine sulfate (0.00008 mg/g mouse). Once the mice were under anesthesia, the eyes were covered with an ophthalmic ointment (Duratears, Alcon Laboratories, Inc., Forth Worth, TX) to prevent against light damage and dehydration. The inner thigh of each leg and the surrounding region were depilated and cleaned with a Betadine (Purdue Frederick Company, Norwalk, CT) wipe followed by an ethanol swab. The Betadine-ethanol cleaning sequence was then repeated 2 more times with short breaks of approximately 20 seconds in between to prevent the animal from becoming hypothermic.

All surgical instruments were sterilized with high-pressure saturated steam at 121°C in an autoclave for around 35 minutes and allowed to cool before surgery. After the depilated area on the animal was cleaned, the animal was placed supine on a warmed surgical stage. A sterile drape covered the animal almost entirely, the inner thighs were exposed through openings in the drape, and the nose and mouth were exposed at the edge of the drape. Viewing through a Zeiss surgical dissecting microscope (Stemi 2000, Carl Zeiss, Inc., Thornwood, NY), on one leg a skin incision less than 5 mm long was made directly along the femoral artery immediately distal to where the epigastric artery branches off. The fascia and fat between the skin and underlying muscle were gently cleared by blunt dissection to expose the artery-vein pair running distal to where the epigastric artery-vein pair branches off of the femoral artery-vein. A separated space of less than 4 mm in length was made between the artery and vein, sufficient for ligature

placement. Special care was taken to leave the nerve running with this vessel pair intact and minimally disturbed. Two sterile pieces of silk sutures (6-0, Deknatel, Inc., Fall River, MA) were then tied at less than 2 mm apart around the separated section of the artery. The artery segment between the two ligatures was then severed with micro dissecting scissors. The skin incision was closed with sutures (5-0 Proline, Ethicon, Somerville, NJ) and the animal was left to recover on a heating pad. As the anesthesia wore off, an I.P. injection of buprenorphine (0.03 ml/animal, Reckitt Benckiser Pharmaceuticals Inc., Richmond, VA) was given, followed by a second dose 8-12 hours later.

5.2.2 Femoral Artery Cannulation

Animals were anesthetized with an I.P injection of ketamine (0.12 mg/g mouse), xylazine (0.012 mg/g mouse), and atropine sulfate (0.00008 mg/g mouse), and the inner thighs of each leg were depilated. After being secured on a warmed surgical stage, a skin incision approximately 1 cm long was made directly along the ligated femoral artery immediately after it branches away from the abdominal aorta. The fascia between the skin and the underlying muscle was gently cleared by blunt dissection to expose the femoral artery-vein pair. Using blunt-tip forceps, the artery and vein were gently separated from each other with the length of separated space limited to approximately 5 cm. Care was taken to leave the nerve running with the vessel pair intact and minimally disturbed. Two pieces of 6-0 black braided silk sutures (Ethicon, Somerville, NJ) were placed under the artery to provide tension as a 20 cm PE-10 tubing (Inner diameter: 0.28 mm, Outer Diameter: 0.61 mm, Becton Dickinson & Co., Sparks, MD) pre-connected to a 30G needle (30G1/2, Precision Gluide, Becton Dickinson & Co., Franklin Lakes, NJ) attached to a syringe of 1% heparin saline was inserted through a small incision into the femoral artery and

tied in place with the sutures. Extra care was taken when inserting the tubing, as the tubing diameter was approximately 3 to 4 times larger in diameter than the femoral artery.

5.2.3 JUGULAR VEIN CANNULATION

The animals were anesthetized with an I.P injection of ketamine (0.12 mg/g mouse), xylazine (0.012 mg/g mouse), and atropine sulfate (0.00008 mg/g mouse), and the neck and inner thigh of each leg were depilated. After being secured on a warmed surgical stage, a skin incision was made along the right jugular vein and the jugular vein was exposed by blunt dissection and carefully separated from the surrounding connective tissue. Two pieces of 6-0 black braided silk sutures (Ethicon, Somerville, NJ) were placed under the jugular vein to provide tension as a 20 cm PE-10 tubing (Inner diameter: 0.28 mm, Outer Diameter: 0.61 mm, Becton Dickinson & Co., Sparks, MD) pre-connected to a 30G needle (30G1/2, Precision Gluide, Becton Dickinson & Co., Franklin Lakes, NJ) attached to a syringe of 1% heparin saline was inserted through a small incision into the jugular vein and tied in place with the sutures.

5.2.4 ULTRASOUND-MICROBUBBLE-MEDIATED NANOPARTICLE DELIVERY

After the cannula was inserted into either the jugular vein or femoral artery, the feet were gently taped to the surgical stage such that the inner thighs were easily accessible. A 1-MHz unfocused transducer (A303S, Olympus NDT Inc., Waltham, MA) with a 0.5-inch (1.27 cm) diameter was positioned with a supporting metal arm over the hindlimb with an approximately 8 mm-thick layer of ultrasound transmission gel (Aquasonic® 100 ultrasound transmission gel, Parker Laboratories, Inc., Fairfield, NJ) between it and the skin surface. Albumin microbubbles (approximately 3.54×10^8 MB/ml stock concentration, mean diameter of 3.53 μm) generously provided by Dr. Alexander Klibanov from the Cardiovascular Medicine Department at the University of Virginia were diluted to approximately 3.54×10^7 MB/ml in 0.9% saline solution

containing 1.53×10^{13} 50 nm red NPs (R50, Fluoro-Max Dyed Red Aqueous Fluorescent Paricles, Thermo Scientific Inc., Waltham, MA) and 1.91×10^{12} 100 nm green NPs (G100, Fluoro-Max Dyed Green Aqueous Fluorescent Paricles, Thermo Scientific Inc., Waltham, MA) with a 1 ml syringe (1 ml Sub-Q 26G⅝, Becton Dickinson & Co., Franklin Lakes, NJ). Special care was taken to draw MBs into the syringe slowly to lessen MB shearing and to replace the MB stock vial head space with high-molecular-weight perfluoropropane gas to minimize stock MB destabilization. Additionally, extra attention was also put on promoting homogenous MB size distribution throughout the syringe by gently rolling and rocking the syringe about its cylindrical and medial axis as larger bubbles might have floated more to lumen edges during the drawing process. The syringe was then carefully connected to the cannula to avoid air bubbles and MBs were infused at a rate of 13.333 μl/min with an infusion pump (Standard infusion Only PHD 22/2000 Syringe Pump, Harvard Apparatus, Holliston, MA) after 0.04 ml of dead space of 1% heparin saline (0.9%) originally in the cannula was cleared with a manual infusion at around 1 ml/min. Based on MB infusion simulations detailed in Chapter 4, a large population of MBs was actually not infused into the mouse due to flotation. The MB concentration introduced into the mouse was actually around 1.22×10^{7} MB/ml with a mean diameter of 1.85 μm.

US pulsing was triggered with a LabView software program (National Instruments, Austin, TX) for 12 minutes. One pulse consisted of 10 bursts, each spaced 100 msec apart, where one burst consisted of 300 consecutive 1-MHz sinusoids of 0.8, 0.3, 0.2, or 0.1 volt peak-to-peak amplitude from a waveform generator (Tektronix AFG-310, Sony Tektronix, Beaverton, OR) depending on the treatment group. A total of 72 pulses were applied during the 12-minute treatment. The waveform signal was amplified by a 55-dB RF power amplifier (model 3100LA, ENI, Inc.) and fed into the transducer. In between each pulse, a 10-second interval allowed for

MB reperfusion into the targeted region. Refer to Figure 3.1B (p. 28) for a diagram of the US pulsing protocol described. Experiments in Chapter 4 measured the system's PNP at approximately 0.7, 0.55, 0.4, or 0.2 MPa respectively at roughly where the gracilis muscle lies. During treatment, 0.16 ml of MB solution was infused into the mouse.

5.2.5 HINDLIMB IMAGING FOR PETECHIAE

After USMB treatment, an anterior-posterior skin incision approximately 2 cm long was made along the saphenous artery on the treated hindlimb. A second lateral-medial skin incision also about 2 cm long was made along the centerline of the GM. The skin was then reflected back by blunt dissection to expose the entire GM. The hindlimb was observed using a macroscope at 5x and 8x, images were taken with a Microfire™ digital camera (Model S99809, Olympus America, Melville, NY) and PictureFrame software (Optronics Corp., Muskogee, OK).

5.2.6 GRACILIS MUSCLE HARVESTING

Prior to muscle harvesting, the animals were euthanized with an injection of pentobarbital sodium solution (0.2ml/mouse). For the jugular vein-cannulated mice, the abdominal aorta was cannulated with a PE-10 tubing (Becton Dickinson & Co., Sparks, MD) and the inferior vena cava was severed to allow for removal of remaining blood with infusions of 5 ml of 2% heparinized Tris-buffered saline with $CaCl_2$, 5 ml of Tris-buffered saline with $CaCl_2$, and 5 ml of paraformaldehyde (PFA) (Sigma, St. Louis, MO) at 1 ml/min with an infusion pump (Standard infusion Only PHD 22/2000 Syringe Pump, Harvard Apparatus, Holliston, MA). For the femoral artery-cannulated mice, the inferior vena cava was severed and through the existing femoral artery cannula 1 ml each of 2% heparinized Tris-buffered saline with $CaCl_2$, Tris-buffered saline with $CaCl_2$, and PFA were infused at 0.09 ml/min. While the 2% heparinized Tris-buffered saline was being infused, the region of the USMB-NP-treated GM between the

saphenous artery and the proximal feeder on the treated leg was carefully dissected free from the underlying muscles. After the blood removal process was completed, about 1 ml of 4% PFA was suffused over the GM and the muscle was left to fix *in situ* for approximately 30 minutes. After fixation, the GM was excised and stored in a 50/50 mixture of PBS and glycerol at -20°C.

GM fixation via perfusion was critical in this study to remove any NP from the vessel lumen. As a result, all NPs observed in the GM sections (see *5.2.9 Gracilis Muscle Cross Section Imaging and Analysis* fore more detail) can be assumed to reside in either the endothelium or the interstitium.

5.2.7 GRACILIS MUSCLE WHOLE MOUNT IMAGING

For imaging, the muscles were mounted on microscopic slides with PBS and temporarily sealed with glass cover slides. GMs were observed with a 4x air objective on a Nikon TE-300 inverted microscope (Nikon, Melville, NY), images were acquired with a Microfire™ digital camera (Model S99809, Olympus America, Melville, NY) and PictureFrame software (Optronics Corp., Muskogee, OK) used in conjunction with a mercury lamp. Using the photomerge function in Photshop CS2 (Adobe Systems Inc., San Jose, CA) composite images of GMs were created from scans of individual regions.

5.2.8 GRACILIS MUSCLE SECTIONING AND STAINING

After the whole mount images were taken, the GMs were dried gently on a Kimwipe® and were bisected about their midlines perpendicular to the longitudinal axes of muscle fibers. With the cut ends of the muscles oriented toward the bottom of sectioning dishes filled with Optimal Cutting Temperature (OCT) compound (Tissue-Tek®, Sakura Finetek U.S.A., Inc., Torrance, CA), the specimens in OCT were left in room temperature for approximately 20 minutes before being frozen in the -80°C freezer.

8-micron thick sections were cut using a cryotome (Leica CM3050 Cryostat, Leica Instruments GmbH, Nussloch, Germany) by Dr. Ji Song from the Biomedical Engineering Department at the University of Virginia, yielding representative sections from both the lateral and medial regions of the fixed muscles. The cryosections were then incubated overnight with 1:140 AlexaFluor®647-conjugated isolectin GS-IB_4 from *Griffonia simplicifolia* (Life Technologies, Inc., Carlsbad, CA) in 0.1% saponin and 2% BSA in PBS at 4°C in a humid chamber. Afterwards the sections were washed in 0.1% saponin and 2% BSA in PBS 2 times 20 minutes each at room temperature, followed by a wash in PBS for 20 minutes in room temperature. The sections were then mounted on a microscopic slide with a mounting medium (VECTASHIELD® Hardset Mounting Medium with DAPI, Vector Laboratories Inc., Burlingame, CA) and a glass coverslip and left in 4°C overnight for the mounting to set.

5.2.9 Gracilis Muscle Cross Section Imaging and Analysis

Mounted USMB-NP-treated GM cross sections were imaged using the Nikon Eclipse C1si confocal microscope system (Nikon, Melville, NY) and the associated control software EZ-C1 (Nikon, Melville, NY) with a 20x oil objective. Images of every field of view within each section were taken at a pixel dwell of 20.40 μs and gain levels at 6.60 for the red and green channels, and 6.40 for the blue channel. Using the photomerge function in Photshop CS2 (Adobe Systems Inc., San Jose, CA), the fields of view for each section were combined into a montage to create a complete image.

The montaged images of sections were analyzed using ImageJ. To determine the total amount of NPs delivered per section, the images of NPs in cross sections were first thresholded to zero out the background and autofluorescence from muscle fibers yielding only NPs within the image. The sections were then manually traced within the image to yield a pixel value per

section, which is representative of the total NP amount delivered per cross section. To calculate the amount of NPs delivered specifically to the endothelium and interstitium, the image calculator function in ImageJ was used. Specifically, thresholded images of endothelium in cross sections were substracted from thresholded images of NPs in cross sections to give images showing NPs in the interstitium per cross section. Those images were then manually traced to get a pixel value presenting the amount of NPs delivered to the interstitium. To get the amount of NPs delivered to the endothelium, the pixel value representing NPs delivered to the interstitium was subtracted from the pixel value representing the total NPs delivered. Two representative sections were analyzed for each mouse.

5.2.10 Statistical Analysis

For the nanoparticle delivery studies, Two-Way ANOVA was performed to analyze the statistical significance of differences between differently sized NPs delivered to different tissue spaces with different US PNP levels. Pairwise multiple comparison procedures were performed using the Holm-Sidak method. Statistical significance was assessed at $p<0.05$. All statistical procedures were performed using SigmaStat version 3.5 (Systat Software Inc., San Jose, CA).

5.3 Results and Discussion

To determine how various US PNPs affect the distribution of NPs delivered by US-MB interactions in ischemic mouse skeletal muscle, PNP levels were applied at 0.7 MPa, 0.55 MPa, 0.4 MPa, and 0.2 MPa with 50 nm red and 100 nm green fluorescent NPs introduced into the mouse either through femoral artery or jugular vein cannulations. Cross sections of the treated GMs stained for lectin to mark endothelial cells were imaged at 20x to visualize NP distribution among the tissue compartments (Figure 5.2, p. 53; Figure 5.3, p. 54). The images were then quantitatively assessed to yield profiles of total amount of NPs delivered per cross section,

amount of NPs delivered specifically to interstitial and endothelial spaces per cross section, proportions of NP delivery to each space, and the percentage of endothelial cells in the cross section containing NPs (Figure 5.4, p. 55; Figure 5.5, p. 56). Additionally, whole mount images of harvested GMs from the femoral artery cannulation route treatment group were taken to demonstrate qualitatively the varying extents of petechiae and NP delivery across the entire muscle at each PNP level applied (Figure 5.1, p. 52).

5.3.1 Nanoparticle Delivery via Femoral Artery Cannulation

For USMB-induced NP delivery via femoral artery cannulations, varying the US PNP level applied was found to affect the total amount of NPs delivered to the skeletal muscle and the distribution of NPs delivered across the endothelial and interstitial spaces (Figure 5.1, p. 52; Figure 5.2, p. 53). NPs delivered to the tissue increased by roughly 2 to 4 fold as PNP increased from the lower levels of 0.2 MPa and 0.4 MPa to the higher levels of 0.55 MPa and 0.7 MPa (Figure 5.4A, p. 55). NPs in the interstitium increased accordingly by approximately 2 to 6 fold from lower to higher pressures, while endothelial NP amounts increased by up to ~2 fold (Figure 5.2, p. 53; Figure 5.4B, p. 55). It seems that the total delivery increase was caused mostly by more and more NPs transferred to the interstitium (Figure 5.2, p. 53). Overall, as PNP increased, the distribution among NPs delivered shifted heavily towards the interstitial space (Figure 5.3, p. 54).

As PNPs increased, the corresponding increases in NP delivery to the interstitium and endothelium were likely the result of larger forces from stronger inertial and noninertial cavitations that increased the cell membrane and blood vessel wall permeabilities to a greater degree. At the higher PNPs, favored promotion of interstitial delivery was possibly caused by powerful cavitational forces that created more and/or larger pores in capillary walls and perhaps

the walls of bigger vessels, which enabled greater amounts of NP transfer into the interstitium by convection. In contrast, forces associated with lower PNPs were likely gentler and created less damage on the vessel wall, which could have possibly opened fewer and smaller pores that were also more transient to permit less NP transfer.

For the smaller amounts of increase seen in endothelial NP delivery over PNP increments compared to that for interstitial delivery, a possible cause may have been limited space within cells for NP occupation upon transport compared to the interstitium. Another may be endothelial cell damage or death caused by US-MB interactions as PNP rose, which could have resulted in fewer cells remaining for NP delivery or those that were delivered with NPs. One other reason considered was the saturation of NPs in the endothelial cells present, which may have discouraged additional NP delivery into the endothelium when pressures increased. However, Figure 5.4D (p. 55) indicates that at most, only about 50% of the endothelial cells contained NPs, which makes evident that the endothelial cells were in fact not saturated.

Based on the results obtained, more tailored USMB-mediated therapeutic agent delivery approaches could be possibly devised for future studies. For example, to direct maximum total transfer of 50 nm NPs to the USMB-targeted tissue or to the interstitial space in particular, PNP applied at 0.55 MPa may be preferred over 0.7 MPa as there are no significant differences in the amount of NPs delivered to the tissue or the interstitium between the two (Figure 5.4A, p.55) while there may be lower risk for unintended and undesirable endothelial cell damage associated with the 0.55 MPa PNP compared to the higher PNP of 0.7 MPa. If an even distribution of 100 nm NPs across the interstitium and endothelium were to be preferred, then a PNP of 0.2 MPa would perhaps be the best option (Figure 5.4 B & C, p. 55).

5.3.2 NANOPARTICLE DELIVERY VIA JUGULAR VEIN CANNULATION

Compared to the femoral artery cannulation route, the jugular vein route delivered around 100 fold less NPs to the tissue at all PNP levels applied, which is evident qualitatively from the lesser amount of NPs observed in GM cross sections (Figure 5.2 vs. 5.3, p. 53 & p. 54) and quantitatively from the average total NP coverages measured per cross section (Figure 5.4A vs. 5.5A, p. 55 & p. 56). This was likely caused by the difference in the average size and number of MBs and number of NPs that reach the US-targeted region delivered via the two routes, as MBs and NPs delivered through the jugular vein route were subject to redistribution by the heart, filtration by the lungs, and longer circulation before arriving at the site of US interaction. We suspect the MB populations to be of smaller average size and number, and that fewer NPs would be present compared to MBs and NPs delivered immediately upstream of the US-treated muscle through femoral artery cannulations.

The total amount of 50 nm NPs delivered through the jugular vein route appeared to increase by about 2 fold when PNP increased from the lower levels of 0.2 MPa and 0.4 MPa to the higher levels of 0.55 MPa and 0.7 MPa (Figure 5.5A, p. 56). Similar to that mentioned in *5.3.1*, the reasons likely involve stronger inertial and noninertial cavitational forces caused by the higher PNPs that increase endothelial cell membrane and blood vessel wall permeabilities to a greater extent. For the 100 nm NPs however, delivery was very low to nearly nonexistent across PNPs where no significant differences were detected in between. Since 50 nm NPs were well transported, we speculate that perhaps the 100 nm NPs were heavily filtered by the liver and a very low concentration of the 100 nm NPs were available in the circulation for potential delivery by US-MB interactions.

Contrary to what was seen in the femoral artery cannulation route group, for 50 nm NPs delivered under 0.2, 0.4 and 0.55 MPa PNPs there were significantly more NP deposits in the

endothelium than the interstitium (Figure 5.5B, p. 56). A possible explanation for this would be that due to the smaller average diameter of MBs present in the circulation, forces generated by inertial and/or noninertial cavitations in response to US were perhaps mostly small enough for cell membrane pore formation or other membrane permeability properties to change but not blood vessel penetration or intercellular gap formation, which would have allowed for NP transport into the endothelial cells but not through the vessel walls and into the interstitial space. At 0.7 MPa PNP however, NP delivery to the interstitium seemed greater than to the endothelium, although the difference was not significant (Figure 5.5B, p. 56). The interstitial NP delivery was significantly greater than that at lower PNPs and was probably caused by stronger forces generated by US-induced MB cavitations sufficient for transport channel generation in the vessel wall. This suggests a probable PNP threshold that exists between 0.7 MPa and 0.55 MPa, which reflects a transition away from pro-endothelium delivery to potentially pro-interstitial delivery possible for the corresponding MB and tissue parameters.

Based on the results obtained, it is apparent that different PNPs may be applied to drive more optimal delivery of NPs to desired tissue spaces. For instance, to direct maximum total transfer of NPs (50 nm NPs) to the whole GM or to the endothelium specifically 0.55 MPa might be best (Figure 5.5A & B, p. 56), whereas for maximized interstitial delivery 0.7 MPa would be a better option (Figure 5.5B, p. 56).

Overall, by harnessing the outcomes acquired from both femoral artery and jugular vein cannulation route directed NP deliveries in this study USMB-mediated transport could be further customized to study the effect of various delivered dosages in desired tissue spaces.

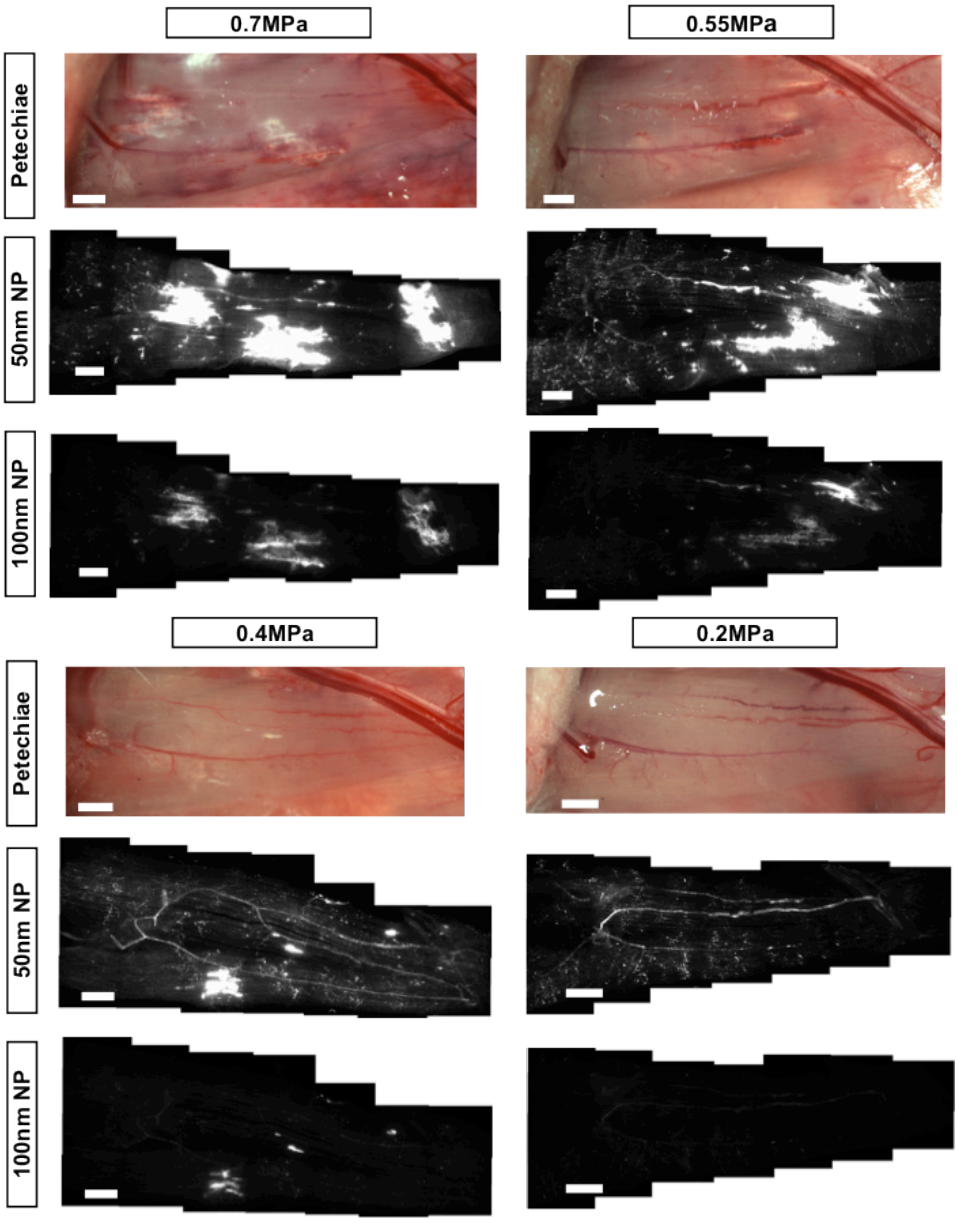

Figure 5.1 Representative whole mount images of USMB-NP-treated gracilis muscles where MBs and NPs were delivered through the femoral artery cannulation route. Scale bar = 1 mm.

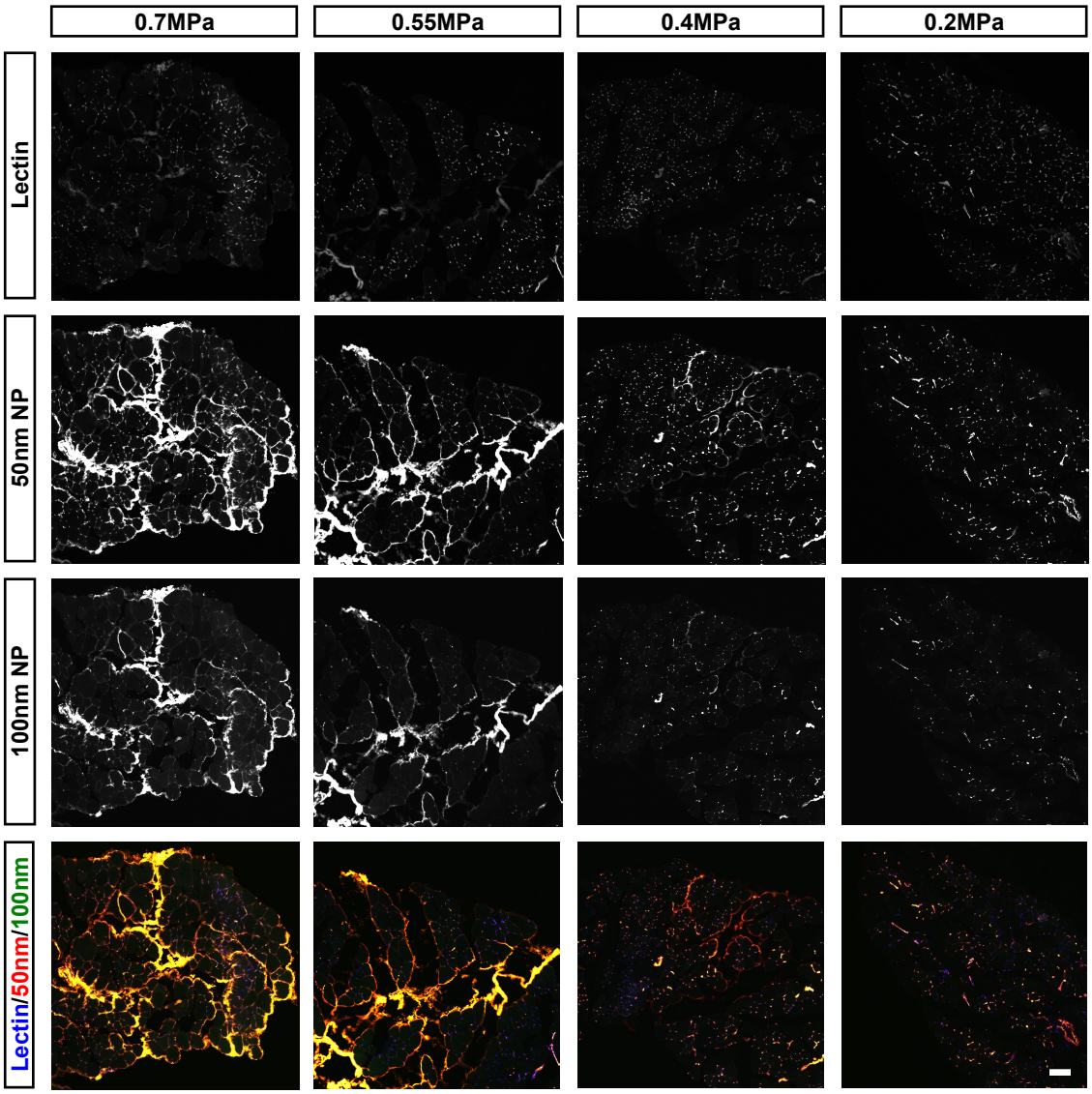

Figure 5.2 Representative 20x confocal microscope scanned fields of view of gracilis mucle sections containing 50 nm and 100 nm NPs delivered through the **femoral artery** cannulation route. Scale bar = 50 μm.

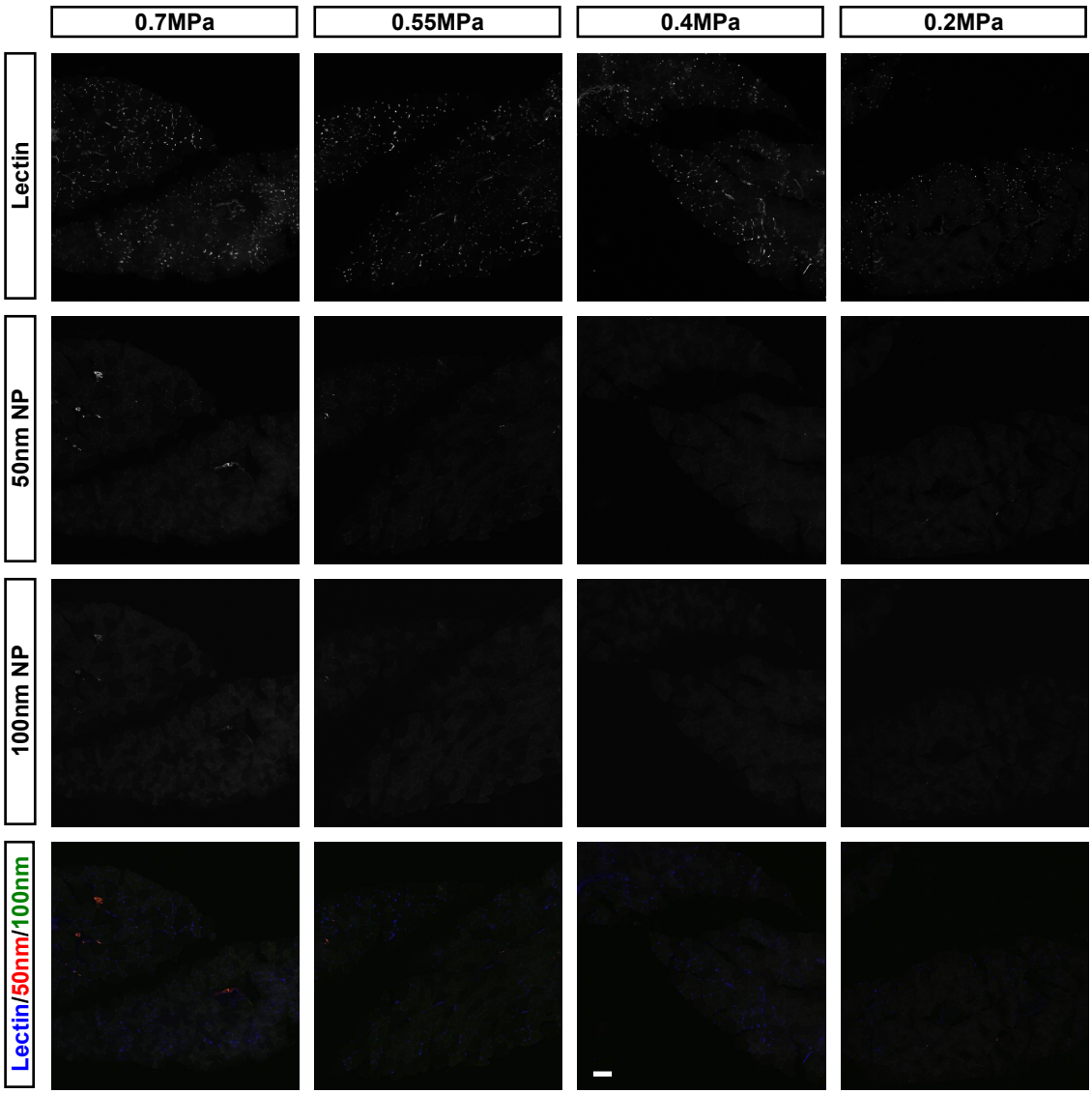

Figure 5.3 Representative 20x confocal microscope-scanned fields of view of gracilis muscle sections containing 50 nm and 100 nm NPs delivered through the **jugular vein** cannulation route. Scale bar = 50 μm.

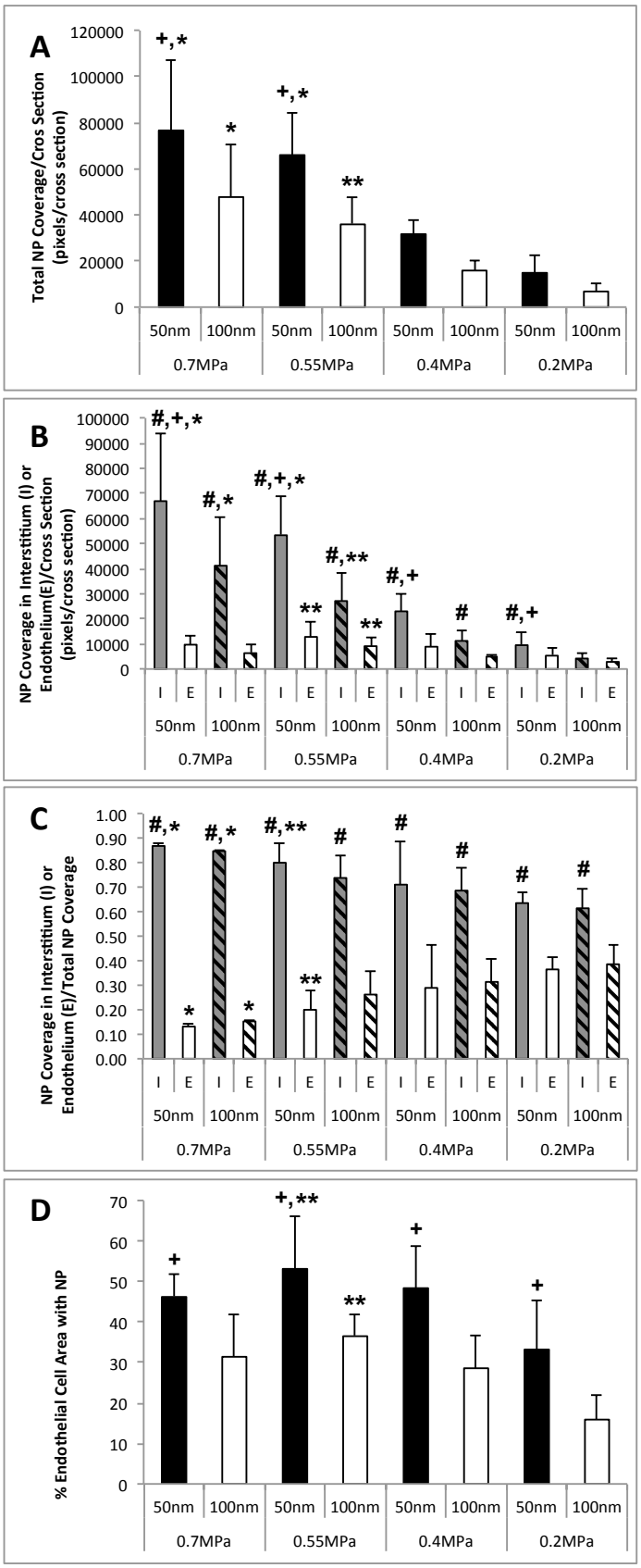

Figure 5.4 Bar graphs showing (A) total NP coverage per cross section, (B) NP coverage in the interstitium or endothelium per cross section , (C) proportion of NP coverage in the interstitium or endothelium out of total NP coverage per cross section, (D) proportion of endothelial cell area with NPs for NPs delivered through the **femoral artery** cannulation route.
(A) + Indicates significantly different than 100 nm NP coverage with the same PNP. * Indicates significantly different than identically-sized NP coverage with PNP of 0.4 MPa and 0.2 MPa. ** Indicates significantly different than 100 nm NP coverage with PNP of 0.2 MPa.
(B) # Indicates significantly different than identically-sized NP coverage in the endothelium with the same PNP. + Indicates significantly different than 100 nm NP coverage in the interstitium with the same PNP. * Indicates significantly different than identically-sized NP coverage in the interstitium with PNP of 0.4 MPa and 0.2 MPa. ** Indicates significantly different than identically-sized NP coverage in the same tissue space with PNP of 0.2 MPa.
(C) # Indicates significantly different than identically-sized NP coverage in the endothelium with the same PNP. * Indicates significantly different than identically-sized NP in the same tissue space with PNP of 0.4 MPa and 0.2 MPa. ** Indicates significantly different than 50 nm NP coverage in the same tissue space with PNP of 0.2 MPa.
(D) + Indicates significantly different than 100 nm NP coverage with the same PNP. ** Indicates significantly different than identically-sized NP coverage with PNP of 0.2 MPa.

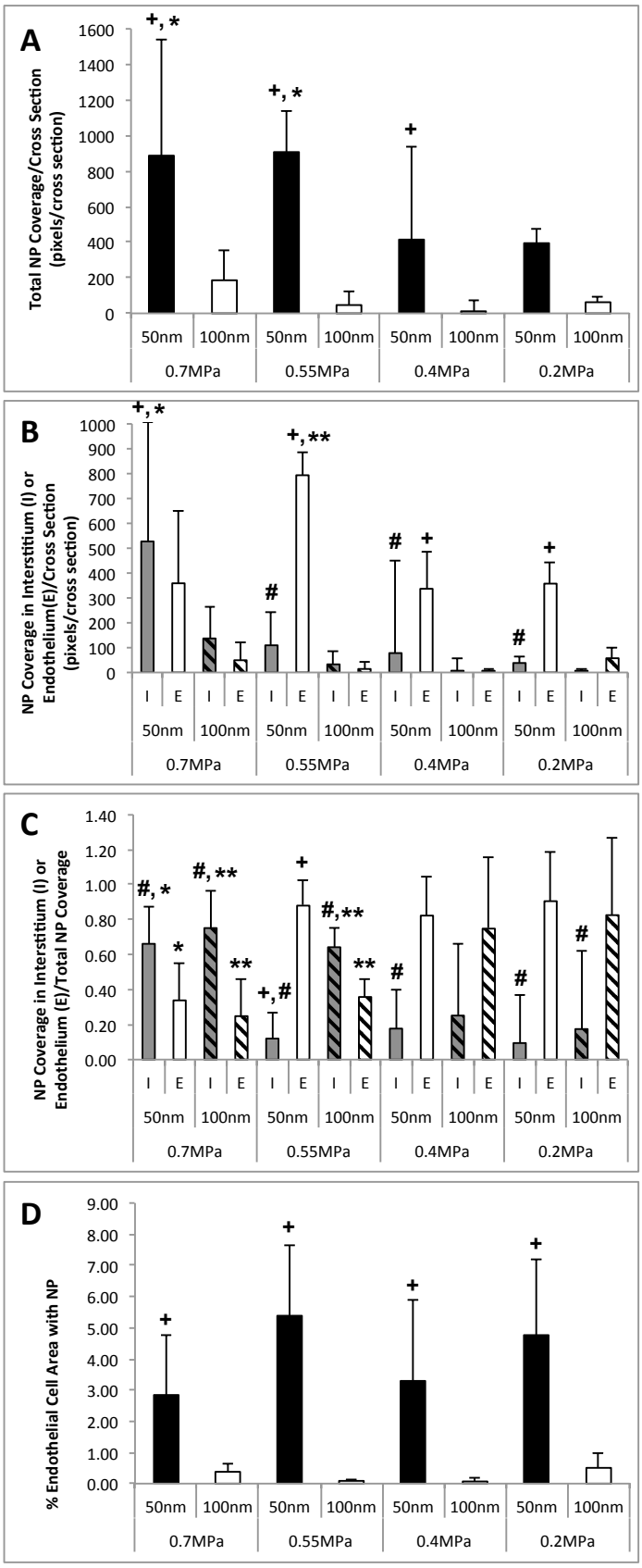

Figure 5.5 Bar graphs showing (A) total NP coverage per cross section, (B) NP coverage in the interstitium or endothelium per cross section, (C) proportion of NP coverage in the interstitium or endothelium out of total NP coverage per cross section, (D) proportion of endothelial cell area with NPs for NPs delivered through the **jugular vein** cannulation route**.**
(A) + Indicates significantly different than 100 nm NP coverage with the same PNP. * Indicates significantly different than 50 nm NP coverage with PNP of 0.4 MPa and 0.2 MPa.
(B) # Indicates significantly different than identically-sized NP coverage in the endothelium with the same PNP. + Indicates significantly different than 100 nm NP coverage in the same tissue space with the same PNP. * Indicates significantly different than 50 nm NP coverage in the interstitium with PNP of 0.55 MPa, 0.4 MPa, and 0.2 MPa. ** Indicates significantly different than 50 nm NP coverage in the endothelium with PNP of 0.7 MPa, 0.4 MPa, and 0.2 MPa.
(C) # Indicates significantly different than identically-sized NP coverage in the endothelium with the same PNP. + Indicates significantly different than 100 NP coverage in the same tissue space with the same PNP. * Indicates significantly different than 50 nm NP coverage in the endothelium with PNP of 0.55 MPa, 0.4 MPa, and 0.2 MPa. ** Indicates significantly different than 100 nm NP coverage in the endothelium with PNP of 0.4 MPa and 0.2 MPa.
(D) + Indicates significantly different than 100 nm NP coverage with the same PNP.

CHAPTER 6: INFLAMMATORY RESPONSE INDUCED BY ULTRASOUND AND MICROBUBBLES

6.1 INTRODUCTION

To determine how various ultrasound (US) peak negative pressures (PNPs) affect the inflammatory response generated by US-MB interactions in ischemic mouse skeletal muscle, PNP levels were applied at 0.7 MPa, 0.55 MPa, 0.4 MPa, and 0.2 MPa. CD45 was the marker of choice in this study for quantifying the extent of inflammation in the muscles.

6.2 EXPERIMENTAL METHODS

40 BALB/c mice (25 grams, 9 – 11 weeks old, Harlan Laboratories, Inc., Dublin, VA) were used in this study. To control for the inflammatory response generated by the femoral artery ligation in the ischemic mouse skeletal muscle, 8 mice were tested in a control group where no USMB-treatment was applied throughout the experiment. 8 mice each were experimented for the US PNP levels of 0.7 MPa, 0.55 MPa, 0.4 MPa, and 0.2 MPa.

For the USMB-treated groups, the experiment time course was femoral artery ligation on day 0, USMB treatment on day 4, USMB-treated GM harvest on day 5. For the control group, it was femoral artery ligation on day 0, femoral artery-ligated GM harvest on day 5. The muscles were paraffin embedded and sectioned, then stained for CD45+ cells. The stained cross sections were imaged and manually counted for number of CD45+ cells per cross section.

6.2.1 FEMORAL ARTERY LIGATION

Mice received unilateral arterial occlusions and were maintained under sterile conditions throughout experimentation. Animals were anesthetized by an I.P. injection of ketamine (0.12 mg/g mouse), xylazine (0.012 mg/g mouse), and atropine sulfate (0.00008 mg/g mouse). Once the mice were under anesthesia, the eyes were covered with an ophthalmic ointment (Duratears,

Alcon Laboratories, Inc., Forth Worth, TX) to prevent against light damage and dehydration. The inner thigh of each leg and the surrounding region were depilated and cleaned with a Betadine (Purdue Frederick Company, Norwalk, CT) wipe followed by an ethanol swab. The Betadine-ethanol cleaning sequence was then repeated 2 more times with short breaks of approximately 20 seconds in between to prevent the animal from becoming hypothermic.

All surgical instruments were sterilized with high-pressure saturated steam at 121°C in an autoclave for around 35 minutes and allowed to cool before surgery. After the depilated area on the animal was cleaned, the animal was placed supine on a warmed surgical stage. A sterile drape covered the animal almost entirely, the inner thighs were exposed through openings in the drape, and the nose and mouth were exposed at the edge of the drape. Viewing through a Zeiss surgical dissecting microscope (Stemi 2000, Carl Zeiss, Inc., Thornwood, NY), on one leg a skin incision less than 5 mm long was made along the femoral artery immediately distal to where the epigastric artery branches off. The fascia and fat between the skin and underlying muscle were gently cleared by blunt dissection to expose the artery-vein pair running distal to where the epigastric artery-vein pair branches off of the femoral artery-vein. A separation of less than 4 mm in length was made between the artery and vein, sufficient for ligature placement. Special care was taken to leave the nerve running with this vessel pair intact and minimally disturbed. Two sterile pieces of silk sutures (6-0, Deknatel, Inc., Fall River, MA) were then tied at less than 2 mm apart around the separated section of the artery. The artery segment between the two ligatures was then severed with micro dissecting scissors. The skin incision was closed with sutures (5-0 Proline, Ethicon, Somerville, NJ) and the animal was left to recover on a heating pad. As the anesthesia wore off, an I.P. injection of buprenorphine (0.03 ml/animal, Reckitt

Benckiser Pharmaceuticals Inc., Richmond, VA) was given, followed by a second dose 8-12 hours later.

6.2.2 JUGULAR VEIN CANNULATION

All surgical instruments were sterilized with high-pressure saturated steam at 121°C in an autoclave for around 35 minutes and allowed to cool before surgery. Animals were anesthetized with an I.P injection of ketamine (0.12 mg/g mouse), xylazine (0.012 mg/g mouse), and atropine sulfate (0.00008 mg/g mouse). The neck and inner thigh of each leg were depilated and the neck region was cleaned with a Betadine wipe followed by an ethanol swab for 3 times. After being secured on a warmed surgical stage, a sterile surgical drape covered the animal almost entirely, the neck was exposed through the opening in the drape, and the nose and mouth were exposed at the edge of the drape. A skin incision was made along the jugular vein on one side and the jugular vein was exposed by blunt dissection and carefully separated from the surrounding connective tissue. Two pieces of 6-0 black braided silk sutures (Ethicon, Somerville, NJ) were placed under the jugular vein to provide tension as a 20 cm PE-10 tubing (Inner diameter: 0.28 mm, Outer Diameter: 0.61 mm, Becton Dickinson & Co., Sparks, MD) connected to a 30G needle (30G1/2, Precision Gluide, Becton Dickinson & Co., Franklin Lakes, NJ) attached to a syringe of 1% heparin saline was inserted through a small incision into the jugular vein and tied in place with the sutures.

6.2.3 ULTRASOUND-MICROBUBBLE APPLICATION

After the cannula was inserted into the jugular vein, the sterile drape section above the legs was lifted away from the legs, and the feet were gently taped to the surgical stage such that the inner thighs were easily accessible. A 1-MHz unfocused transducer (A303S, Olympus NDT Inc., Waltham, MA) with a 0.5-inch (1.27 cm) diameter was positioned with a supporting metal

arm over the hindlimb with an approximately 8 mm-thick layer of ultrasound transmission gel (Aquasonic® 100 ultrasound transmission gel, Parker Laboratories, Inc., Fairfield, NJ) between it and the skin surface. Albumin microbubbles (approximately 3.54×10^8 MB/ml stock concentration, mean diameter of 3.53 μm) generously provided by Dr. Alexander Klibanov from the Cardiovascular Medicine Department at the University of Virginia were diluted to approximately 3.54×10^7 MB/ml in sterile 0.9% saline solution with a 1 ml syringe (1 ml Sub-Q 26G⅝, Becton Dickinson & Co., Franklin Lakes, NJ). Special care was taken to draw MBs into the syringe slowly to lessen MB shearing and to replace the MB stock vial head space with high-molecular-weight perfluoropropane gas to minimize stock MB destabilization. Additionally, extra attention was also put on promoting homogenous MB size distribution throughout the syringe by gently rolling and rocking the syringe about its cylindrical and medial axis as larger bubbles might have floated more to lumen edges during the drawing process. The syringe was then carefully connected to the cannula to avoid air bubbles and MBs were infused at a rate of 13.333 μl/min with an infusion pump (Standard infusion Only PHD 22/2000 Syringe Pump, Harvard Apparatus, Holliston, MA) after 0.04 ml of dead space of 1% heparin saline (0.9%) originally in the cannula was cleared with a manual infusion at a rate of around 1 ml/min. Based on MB infusion simulations detailed in Chapter 4, a large population of MBs was actually not infused into the mouse as assumed due to flotation, hence the actual concentration introduced into the mouse was around 1.22×10^7 MB/ml with a mean diameter of 1.85 μm.

US pulsing was triggered with a LabView software program (National Instruments, Austin, TX) for 12 minutes. One pulse consisted of 10 bursts, each spaced 100 msec apart, where one burst consisted of 300 consecutive 1-MHz sinusoids of 0.8, 0.3, 0.2, or 0.1 volt peak-to-peak amplitude from a waveform generator (Tektronix AFG-310, Sony Tektronix, Beaverton,

OR) depending on the treatment group. 72 pulses were applied during the 12-minute treatment. The waveform signal was amplified by a 55-dB RF power amplifier (model 3100LA, ENI, Inc.) and fed into the transducer. In between each pulse, a 10-second interval allowed for MB reperfusion into the targeted region. Refer to Figure 3.1B (p. 28) for a diagram of the US pulsing protocol described. Experiments in Chapter 4 measured the system's peak negative pressure as approximately 0.7, 0.55, 0.4, or 0.2 MPa respectively at roughly where the gracilis muscle lies. During treatment, 0.16 ml of MB solution was infused into the mouse.

After the USMB treatment, a piece of 6-0 black braided silk suture (Ethicon, Somerville, NJ) was placed under the jugular vein distal to the two cannula-securing sutures and used to tie off the jugular vein once the cannula was removed. The skin incision was then closed using 5-0 Proline sutures (Ethicon, Somerville, NJ). As the anesthesia wore off, animals were given an I.P. injection of buprenorphine (0.03 ml/animal, Reckitt Benckiser Pharmaceuticals Inc., Richmond, VA). A second dose was administered 8 to 12 hours later and the animals were allowed to recover.

6.2.4 GRACILIS MUSCLE HARVESTING AND STAINING

24 hours after USMB treatment, the treated GM was harvested. For the control group, muscles were harvested on day 5 after femoral artery ligation to match the USMB treatment groups. The animals were euthanized with an injection of pentobarbital sodium solution (0.2ml/mouse). The abdominal aorta was cannulated with a PE-10 tubing (Becton Dickinson & Co., Sparks, MD) and the inferior vena cava was severed to allow for removal of remaining blood with infusions of 5 ml of 2% heparinized Tris-buffered saline with $CaCl_2$, 5 ml of Tris-buffered saline with $CaCl_2$, and 5 ml of 10% formalin (Fisher Scientific, Pittsburgh, PA) at 1 ml/min with an infusion pump (Standard infusion Only PHD 22/2000 Syringe Pump, Harvard

Apparatus, Holliston, MA). While the 2% heparinized Tris-buffered saline was being infused, the region of the USMB-treated GM between the saphenous artery and the proximal feeder on the treated leg was carefully dissected free from the underlying muscles. After the blood removal process was completed, about 1 ml of 10% formalin was suffused over the GM and the muscle was left to fix *in situ* for approximately 30 minutes. After fixation, the GM was excised and placed in histology cassettes in 10% formalin at room temperature until embedded in paraffin and sectioned.

All the USMB-treated muscles were sent to the Research Histology Core at the University of Virginia for embedding in paraffin and sectioning at 5-microns thick per section. The sections were then sent to the Biorepository and Tissue Research Facility at the University of Virginia for immunoenzyme staining for CD45+ cells using a DAKO Autostainer. Briefly, the staining protocol involved using the primary antibody rat anti-mouse CD45 (550539, BD Pharmingen, San Jose, CA) diluted 1:80 in DAKO Antibody Diluent, secondary antibody biotin-conjugated rabbit anti-rat diluted at 1:200, a detection reagent streptavidin-conjugated horseradish peroxidase diluted at 1:200, chromagen DAKO DAB+ substrate, and counterstain hematoxylin. The sections were then mounted on a microscopic slide with a mounting medium and a glass coverslip.

6.2.5 GRACILIS MUSCLE CROSS SECTION IMAGING

Images of every field of view within each section were taken with a 20x air objective on a Nikon TE-300 inverted microscope (Nikon, Melville, NY) and images were acquired with a Microfire™ digital camera (Model S99809, Olympus America, Melville, NY) and PictureFrame software (Optronics Corp., Muskogee, OK). Using the photomerge function in Photshop CS2

(Adobe Systems Inc., San Jose, CA), the fields of view for each section were montaged to create a complete image (Figure 6.1, p. 64).

6.2.6 Gracilis Muscle Cross Section Analysis

The cell counter plugin in ImageJ was used to manually tally the number of CD45+ cells per section (Figure 6.1). Two representative cross sections were analyzed per mouse.

6.2.7 Statistical Analysis

Data on the number of CD45+ cells per section failed the normality test hence a Kruskal-Wallis One-Way ANOVA was performed. Statistical significance was assessed at $p<0.05$. Statistical procedures were performed using SigmaStat version 3.5 software (Systat Software Inc., San Jose, CA).

6.3 Results and Discussion

To determine how various US PNPs affect the inflammatory response generated by US-MB interactions in ischemic mouse skeletal muscle, PNP levels were applied at 0.7 MPa, 0.55 MPa, 0.4 MPa, and 0.2 MPa. The inflammatory response was quantified by manually tallying the number of CD45+ cells present in GM cross sections (Figure 6.1, p. 64; Figure 6.2, p. 65). Statistical analysis of the results acquired suggest no significant differences across all treatment groups, which indicates that variations in PNPs applied in USMB treated ischemic mouse skeletal muscles do not significantly alter the inflammatory responses. However, the power of the test was only at 0.13, much lower than the standard of 0.8. This implies that the statistical test was very weak and that the findings are thus not quite conclusive. To improve the weight of the results, more mice would likely need to be experimented for each treatment group.

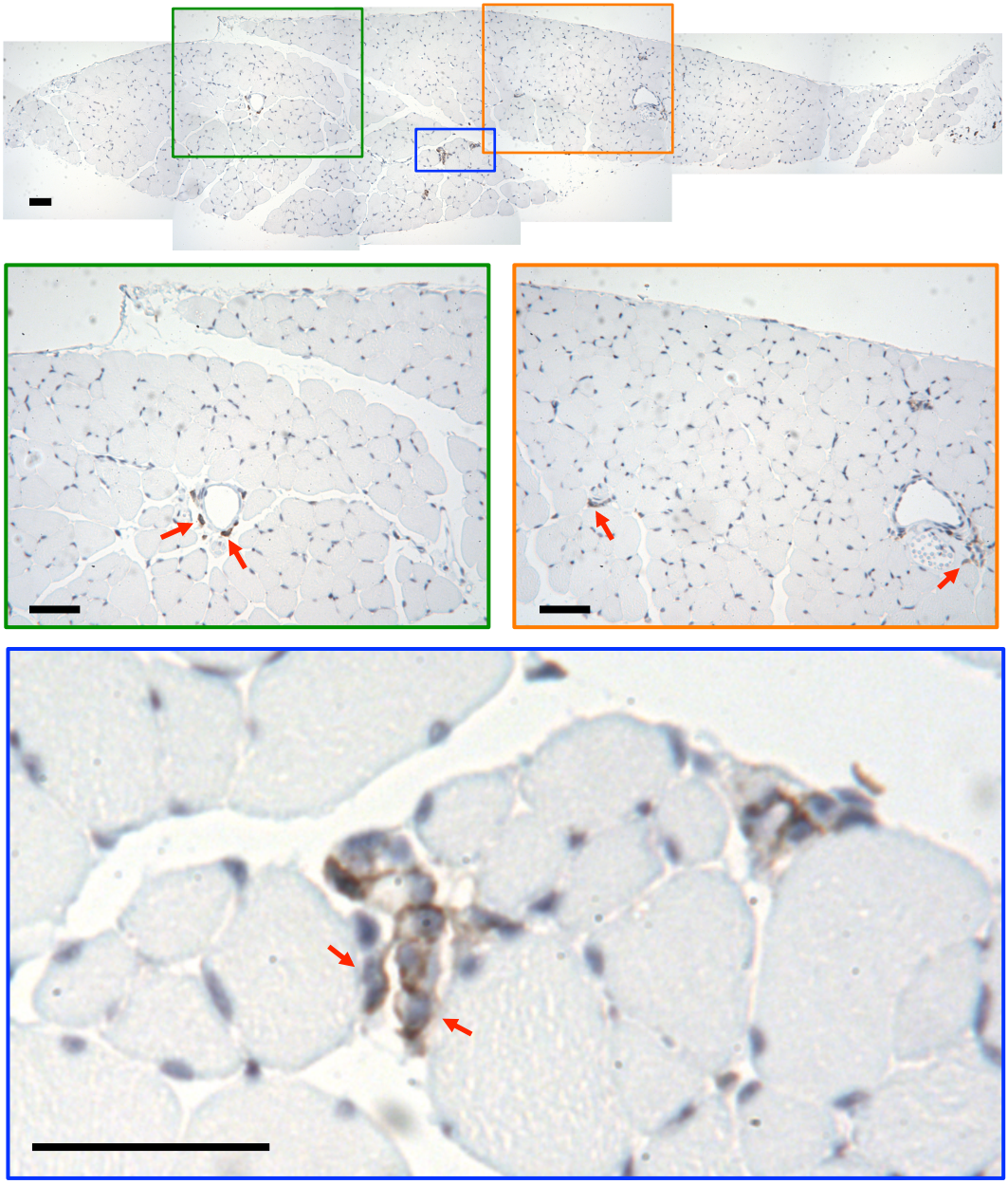

Figure 6.1 Sample gracilis muscle cross section stained for CD45 and hematoxylin. Red arrows point to some of the CD45+ cells counted in each section. Scale bar = 50 µm.

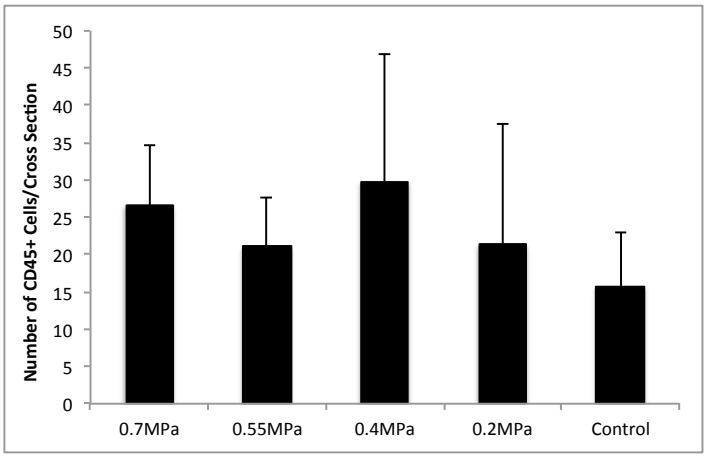

Figure 6.2 Bar graphs showing the number of CD45+ cells per cross section, i.e. the extent of inflammatory response, with respect to each US PNP level applied. No significant difference was detected between the treatment groups.

CHAPTER 7: CONCLUSIONS AND FUTURE STUDIES

7.1 CONCLUSIONS

To determine how various ultrasound peak negative pressures (PNPs) affect the distribution of nanoparticles (NPs) delivered by ultrasound (US)-microbubble(MB) interactions in ischemic mouse skeletal muscle, we tested pressures at 0.7 MPa, 0.55 MPa, 0.4 MPa, and 0.2 MPa with MBs and NPs of 50 nm and 100 nm in diameter introduced into mice either through femoral artery cannulations or jugular vein cannulations. For both cannulation routes we found that increasing the PNP applied generally increased the total amount of NPs delivered to the muscle. For the femoral artery route, increased PNP resulted in increased delivery mostly to the interstitium for both NP sizes. For the jugular vein route, increased delivery mostly to the endothelium as PNP increased up to 0.55 MPa was seen for 50 nm NPs. Overall, we conclude that in coordination with MB concentration and size distribution delivered, adjusting the US PNP applied could be feasible approach for improving the targeting specificity of NP delivery into the tissue.

To measure the inflammatory response generated by ultrasound-microbubble interactions in ischemic mouse skeletal muscle with various levels of ultrasound peak negative pressures applied, we quantified the number of CD45+ cells in muscle cross sections. The results implied no significant differences in inflammatory response across the ultrasound peak negative pressures of 0.7 MPa, 0.55 MPa, 0.4 MPa, and 0.2 MPa applied, but as the power of the statistical test was very low the finding remains inconclusive.

7.2 Future Directions

7.2.1 Effect of Peak Negative Pressures < 0.2 MPa

Based on Figure 5.4C (p. 55), with decreasing PNP, the proportions of NP distributions in the endothelium and interstitium seem to be heading towards the 50% midline of even distribution. For future studies, it would be advantageous to explore further into PNPs lower than 0.2 MPa to see if the NP distribution proportions would possibly reverse or reach a state where exclusive delivery to the endothelium is possible. Such an exclusive state of NP delivery would be beneficial for refining the targeted agent delivery capabilities of US and MB-facilitated therapeutic delivery.

7.2.2 Longer Time Course for Inflammatory Response Study

The US-MB-induced inflammatory response was measured 24 hours after treatment. The inflammatory response to muscle tissue injury however, can actually occur for over two weeks with the rise and fall in recruitment of a number of inflammatory cells such as neutrophils, macrophages, and T lymphocytes (Smith, Kruger, Smith, & Myburgh, 2008). It could be favorable to measure the inflammatory response over several time points for a longer period of time to get a more accurate and holistic account of inflammation in the muscle in response to US-MB interactions.

7.2.3 Delivery using Monodispersed or Less Polydispersed Microbubbles

The diameter of a MB is one of the parameters that determine whether it undergoes inertial or noninertial cavitation under a level of US pressure applied and hence the bioeffects it creates. With the use of monodispersed or less polydispersed microbubbles, the effects that various adjustable parameters studied, such as PNP, may have on bioeffects and agent delivery in US-MB-mediated therapeutics can be better studied.

APPENDICES

APPENDIX A. SAMPLE HIMBLIMB LASER DOPPLER IMAGES AT VARIOUS AMPLIFICATION SETTINGS

A number of amplification settings were tested on several mice pre-, post-ligation and days following to acquire intensity readings of the greatest dynamic range to better capture hindlimb reperfusion. The sample images shown below suggest that an amplification setting of 2x gives a good range of coverage from low to high intensities throughout the image with minimal saturation.

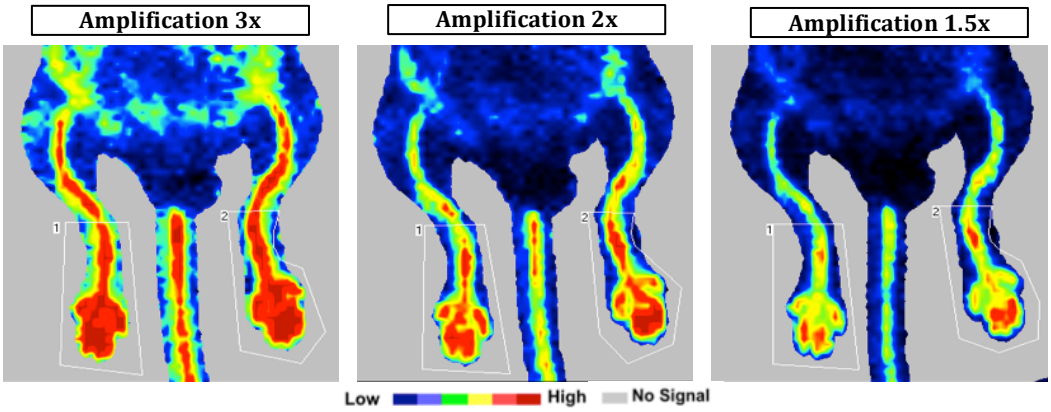

APPENDIX B. MICROFIL INJECTION PROTOCOL FOR MOUSE HINDLIMBS

After the mouse was euthanized by lethal injection of pentobarbital sodium solution (0.2ml/mouse), the abdominal aorta was cannulated with a PE-10 tubing (Becton Dickinson & Co., Sparks, MD) immediately with the inferior vena cava severed for blood removal. A series of solutions were then infused manually through the cannula in the following manner: 10ml of 1% heparinized saline solution (0.9%), 3ml of 4% paraformaldehyde (PFA) (Sigma, St. Louis, MO), 5-minute wait, 3ml of 4% PFA (Sigma, St. Louis, MO), 30-minute wait, 0.8ml of Microfil, and 90-minute wait. Heparinized saline and PFA were infused at approximately 1ml/min and Microfil was infused at about 0.1/min. The mouse is then left in a 4°C environment overnight before scanning with the μCT system (SCANCO Medical, Switzerland). This entire procedure was performed by Dr. Ji Song from the Biomedical Engineering Department at the University of Virginia in this project.

REFERENCES

Balkwill, F., & Mantovani, A. (2001). Inflammation and cancer: back to Virchow? *The Lancet*, *357*(9255), 539–545.

Bergmann, C. E., Hoefer, I. E., Meder, B., Roth, H., Van Royen, N., Breit, S. M., Jost, M. M., et al. (2006). Arteriogenesis depends on circulating monocytes and macrophage accumulation and is severely depressed in op/op mice. *Journal of Leukocyte Biology*, *80*(1), 59–65.

Bobek, V., Taltynov, O., Pinterova, D., & Kolostova, K. (2006). Gene therapy of the ischemic lower limb--Therapeutic angiogenesis. *Vascular pharmacology*, *44*(6), 395–405.

Boutayeb, A., & Boutayeb, S. (2005). The burden of non communicable diseases in developing countries. *International Journal for Equity in Health*, *4*(1), 2.

Browning, R. J., Mulvana, H., Tang, M., Hajnal, J. V., Wells, D. J., & Eckersley, R. J. (2011). Influence of Needle Gauge On In Vivo Ultrasound and Microbubble-Mediated Gene Transfection. *Ultrasound in Medicine and Biology*, *37*(9), 1531–1537.

Burke, C. W., Hsiang, Y. J., Alexander, E., IV, Klibanov, A. L., & Price, R. J. (2011). Covalently Linking Poly(lactic-co-glycolic acid) Nanoparticles to Microbubbles Before Intravenous Injection Improves their Ultrasound-Targeted Delivery to Skeletal Muscle. *Small*, *7*(9), 1227–1235.

Calliada, F., Campani, R., Bottinelli, O., Bozzini, A., & Sommaruga, M. G. (1998). Ultrasound contrast agents: basic principles. *European Journal of Radiology*, *27*, S157–S160.

Caskey, C., Stieger, S., Qin, S., Dayton, P., & Ferrara, K. (2007). Direct observations of ultrasound microbubble contrast agent interaction with the microvessel wall. *The Journal of the Acoustical Society of America*, *122*(2), 1191–1200.

Chalothorn, D., & Faber, J. E. (2010). Strain-dependent variation in collateral circulatory

function in mouse hindlimb. *Physiological genomics*, *42*(3), 469–479.

Chappell, J. C., Klibanov, A. L., & Price, R. J. (2005). Ultrasound-microbubble-induced neovascularization in mouse skeletal muscle. *Ultrasound in Medicine and Biology*, *31*(10), 1411–1422.

Chappell, J. C., & Price, R. J. (2006). Targeted therapeutic applications of acoustically active microspheres in the microcirculation. *Microcirculation*, *13*(1), 57–70.

Chappell, J. C., Song, J., Burke, C. W., Klibanov, A. L., & Price, R. J. (2008a). Targeted delivery of nanoparticles bearing fibroblast growth factor-2 by ultrasonic microbubble destruction for therapeutic arteriogenesis. *Small*, *4*(10), 1769–1777.

Chappell, J. C., Song, J., Klibanov, A. L., & Price, R. J. (2008b). Ultrasonic microbubble destruction stimulates therapeutic arteriogenesis via the CD18-dependent recruitment of bone marrow-derived cells. *Arteriosclerosis, Thrombosis, and Vascular Biology*, *28*(6), 1117–1122.

Chen, W. S., Brayman, A. A., Matula, T. J., Crum, L. A., & Miller, M. W. (2003). The pulse length-dependence of inertial cavitation dose and hemolysis. *Ultrasound in Medicine and Biology*, *29*(5), 739–748.

Clement, D. (2008). Critical limb ischemia. Retrieved August 3, 2011, from www.tasc-2-pad.org

Collis, J., Manasseh, R., Liovic, P., Tho, P., Ooi, A., Petkovic-Duran, K., & Zhu, Y. (2010). Cavitation microstreaming and stress fields created by microbubbles. *Ultrasonics*, *50*(2), 273–279.

de Jong, N., Bouakaz, A., & Frinking, P. (2002). Basic acoustic properties of microbubbles. *Echocardiography*, *19*(3), 229–240.

Dijkmans, P. A., Juffermans, L. J. M., Musters, R. J. P., van Wamel, A., Cate, ten, F. J., van

Gilst, W., Visser, C. A., et al. (2004). Microbubbles and ultrasound: from diagnosis to therapy. *European journal of echocardiography*, *5*(4), 245–256.

Epstein, S. E., Kornowski, R., Fuchs, S., & Dvorak, H. F. (2001). Angiogenesis therapy: amidst the hype, the neglected potential for serious side effects. *Circulation*, *104*(1), 115–119.

Fan, Z., Kumon, R. E., Park, J., & Deng, C. X. (2010). Intracellular delivery and calcium transients generated in sonoporation facilitated by microbubbles. *Journal of Controlled Release*, *142*(1), 31–39.

Feshitan, J., Chen, C., Kwan, J., & Borden, M. (2009). Microbubble size isolation by differential centrifugation. *Journal of Colloid and Interface Science*, *329*(2), 316–324.

Fox, J., Barthold, S., Davisson, M., Newcomer, C., Quimby, F., & Smith, A. (2009). *The mouse in biomedical research* (Vol. 3). Burlington, MA

Gornik, H. (2009). Re-thinking the morbidity of peripheral arterial disease and the "normal" ankle-brachial index. *J Am Coll Cardiol,* 53, 1063-1064.

Harris, K. (2008). The worldwide burden of peripheral artery disease. Retrieved August 3, 2011, from www.tasc-2-pad.org

Helisch, A., Wagner, S., Khan, N., Drinane, M., Wolfram, S., Heil, M., et al. (2005). Impact of Mouse Strain Differences in Innate Hindlimb Collateral Vasculature. *Arteriosclerosis, Thrombosis, and Vascular Biology*, *26*(3), 520–526.

Heil, M., Eitenmüller, I., Schmitz-Rixen, T., & Schaper, W. (2006). Arteriogenesis versus angiogenesis: similarities and differences. *Journal of cellular and molecular medicine*, *10*(1), 45–55.

Henry, T. D. (2003). The VIVA Trial: Vascular Endothelial Growth Factor in Ischemia for Vascular Angiogenesis. *Circulation*, *107*(10), 1359–1365.

Herold, J., Pipp, F., Fernandez, B., Xing, Z., Heil, M., Tillmanns, H., & Braun-Dullaeus, R. C. (2004). Transplantation of monocytes: a novel strategy for in vivo augmentation of collateral vessel growth. *Human Gene Therapy*, *15*(1), 1–12.

Iba, O., Matsubara, H., Nozawa, Y., Fujiyama, S., Amano, K., Mor, Y. et al. (2002). Angiogenesis by Implantation of Peripheral Blood Mononuclear Cells and Platelets Into Ischemic Limbs. *Circulation*, *106*(15), 2019–2025.

Imada, T., Tatsumi, T., Mori, Y., Nishiue, T., Yoshida, M., Masaki, H., et al. (2005). Targeted Delivery of Bone Marrow Mononuclear Cells by Ultrasound Destruction of Microbubbles Induces Both Angiogenesis and Arteriogenesis Response. *Arteriosclerosis, Thrombosis, and Vascular Biology*, *25*(10), 2128–2134.

Juffermans, L. J. M., van Dijk, A., Jongenelen, C. A. M., Drukarch, B., Reijerkerk, A., de Vries, H. E., Kamp, O., et al. (2009). Ultrasound and microbubble-induced intra- and intercellular bioeffects in primary endothelial cells. *Ultrasound in Medicine and Biology*, *35*(11), 1917–1927.

Kalka, C., Masuda, H., Takahashi, T., Kalka-Moll, W. M., Silver, M., Kearney, M., Li, T., et al. (2000). Transplantation of ex vivo expanded endothelial progenitor cells for therapeutic neovascularization. *Proceedings of the National Academy of Sciences*, *97*(7), 3422–3427.

Kaplan, N. M., Palmer, B. F., Bekeredjian, R., & Shohet, R. V. (2004). Cardiovascular gene therapy: angiogenesis and beyond. *The American journal of the medical sciences*, *327*(3), 139.

Klibanov, A. (2006). Microbubble contrast agents: targeted ultrasound imaging and ultrasound-assisted drug-delivery applications. *Investigative Radiology, 41*(3), 354-362.

Kobulnik, J., Kuliszewski, M. A., Stewart, D. J., Lindner, J. R., & Leong-Poi, H. (2009).

Comparison of gene delivery techniques for therapeutic angiogenesis ultrasound-mediated destruction of carrier microbubbles versus direct intramuscular injection. *Journal of the American College of Cardiology*, *54*(18), 1735–1742.

Kondo, I., Ohmori, K., Oshita, A., Takeuchi, H., Fuke, S., Shinomiya, K., Noma, T., et al. (2004). Treatment of Acute Myocardial Infarction by Hepatocyte Growth Factor Gene Transfer. *Journal of the American College of Cardiology*, *44*(3), 644–653.

Kornowski, R., Fuchs, S., Leon, M. B., & Epstein, S. E. (2000). Delivery strategies to achieve therapeutic myocardial angiogenesis. *Circulation*, *101*(4), 454–458.

Lawrie, A., Brisken, A., Francis, S., Wyllie, D., Kiss-Toth, E., Qwarnstrom, E., Dower, S., et al. (2003). Ultrasound-enhanced transgene expression in vascular cells is not dependent upon cavitation-induced free radicals. *Ultrasound in Medicine and Biology*, *29*(10), 1453–1462.

Liu, X., & Wu, J. (2008). Acoustic microstreaming around an isolated encapsulated microbubble. *The Journal of the Acoustical Society of America*, *125*(3), 1319.

Losordo, D. W. (2004). Therapeutic Angiogenesis and Vasculogenesis for Ischemic Disease: Part II: Cell-Based Therapies. *Circulation*, *109*(22), 2692–2697.

Lum, A. F. H., Borden, M. A., Dayton, P. A., Kruse, D. E., Simon, S. I., & Ferrara, K. W. (2006). Ultrasound radiation force enables targeted deposition of model drug carriers loaded on microbubbles. *Journal of Controlled Release*, *111*(1-2), 128–134.

Matoba, S., Tatsumi, T., Murohara, T., Imaizumi, T., Katsuda, Y., Ito, M., Saito, Y., et al. (2008). Long-term clinical outcome after intramuscular implantation of bone marrow mononuclear cells (Therapeutic Angiogenesis by Cell Transplantation [TACT] trial) in patients with chronic limb ischemia. *American Heart Journal*, *156*(5), 1010–1018.

Mayer, C. R., & Bekeredjian, R. (2008). Ultrasonic gene and drug delivery to the cardiovascular

system. *Advanced drug delivery reviews*, *60*(10), 1177–1192.

Meijering, B. D. M., Juffermans, L. J. M., van Wamel, A., Henning, R. H., Zuhorn, I. S., Emmer, M., Versteilen, A. M. G., et al. (2009). Ultrasound and Microbubble-Targeted Delivery of Macromolecules Is Regulated by Induction of Endocytosis and Pore Formation. *Circulation Research*, *104*(5), 679–687.

Miller, D. L., & Chunyan, D. (2004). Membrane damage thresholds for 1-to 10-MHz pulsed ultrasound exposure of phagocytic cells loaded with contrast agent gas bodies in vitro. *Ultrasound in Medicine and Biology*, *30*(7), 973–977.

Miller, D. (2007). WFUMB Safety Symposium on Echo-Contrast Agents: in vitro bioeffects. *Ultrasound in Medicine and Biology*, *33*(2), 197–204.

Miller, D., Averkiou, M., Brayman, A., Everbach, E., Holland, C., Wible, J., Jr, & Wu, J. (2008). Bioeffects considerations for diagnostic ultrasound contrast agents. *Journal of Ultrasound in Medicine*, *27*(4), 611–632.

Miller, D., & Quddus, J. (2000). Diagnostic ultrasound activation of contrast agent gas bodies induces capillary rupture in mice. *Proceedings of the National Academy of Sciences*, *97*(18), 10179–10184.

Mitragotri, S. (2005). Healing sound: the use of ultrasound in drug delivery and other therapeutic applications. *Nature Reviews Drug Discovery*, *4*(3), 255–260.

Morgan, K. E., Allen, J. S., Dayton, P. A., Chomas, J. E., Klibaov, A., & Ferrara, K. W. (2000). Experimental and theoretical evaluation of microbubble behavior: Effect of transmitted phase and bubble size. *Ultrasonics, Ferroelectrics and Frequency Control, IEEE Transactions on*, *47*(6), 1494–1509.

Nakagami, H. (2005). Novel Autologous Cell Therapy in Ischemic Limb Disease Through

Growth Factor Secretion by Cultured Adipose Tissue-Derived Stromal Cells. *Arteriosclerosis, Thrombosis, and Vascular Biology*, *25*(12), 2542–2547.

Nyborg, W. (2007). WFUMB Safety Symposium on Echo-Contrast Agents: mechanisms for the interaction of ultrasound. *Ultrasound in Medicine and Biology*, *33*(2), 224.

Ono, M. (2008). Molecular links between tumor angiogenesis and inflammation: inflammatory stimuli of macrophages and cancer cells as targets for therapeutic strategy. *Cancer Science*, *99*(8), 1501–1506.

Palmer-Kazen, U., Wariaro, D., Luo, F., & Wahlberg, E. (2004). Vascular endothelial cell growth factor and fibroblast growth factor 2 expression in patients with critical limb ischemia. *Journal of Vascular Surgery*, *39*(3), 621–628.

Pitt, W. G., Husseini, G. A., & Staples, B. J. (2004). Ultrasonic drug delivery--a general review. *Expert opinion on drug delivery*, *1*(1), 37–56.

Prentice, P., Cuschieri, A., Dholakia, K., Prausnitz, M., & Campbell, P. (2005). Membrane disruption by optically controlled microbubble cavitation. *Nature Physics*, *1*(2), 107–110.

Price, R. J., & Kaul, S. (2002). Contrast ultrasound targeted drug and gene delivery: an update on a new therapeutic modality. *Journal of Cardiovascular Pharmacology and Therapeutics*, *7*(3), 171–180.

Price, R. J., Skyba, D. M., Kaul, S., & Skalak, T. C. (1998). Delivery of colloidal particles and red blood cells to tissue through microvessel ruptures created by targeted microbubble destruction with ultrasound. *Circulation*, *98*(13), 1264–1267.

Roger, V., Go, A., Lloyd-Jones, D., Adams, R., Berry, J., Brown, T., et al. (2011). Heart disease and stroke statistics--2011 update: A report from the American heart association. *Circulation, 123*(4), e18–e209.

Samuel, S., Cooper, M., Bull, J., Fowlkes, J., & Miller, D. (2009). An Ex Vivo Study of the Correlation between Acoustic Emission and Microvascular Damage. *Ultrasound in Medicine and Biology*, 35(9), 1574–1586.

Sedighiani, F. & Nikol, S. (2011). Gene therapy in vascular disease. *The Surgeon,* 9(6), 326-335.

Sirsi, S., Feshitan, J., Kwan, J., Homma, S., & Borden, M. (2010). Effect of Microbubble Size On Fundamental Mode High Frequency Ultrasound Imaging In Mice. *Ultrasound in Medicine and Biology*, *36*(6), 935–948.

Smith, C., Kruger, M. J., Smith, R. M., & Myburgh, K. H. (2008). The inflammatory response to skeletal muscle injury: illuminating complexities. *Sports Medicine (Auckland, N.Z.)*, *38*(11), 947–969.

Song, J., Chappell, J. C., Qi, M., VanGieson, E. J., Kaul, S., & Price, R. J. (2002). Influence of injection site, microvascular pressure and ultrasound variables on microbubble-mediated delivery of microspheres to muscle. *Journal of the American College of Cardiology*, *39*(4), 726–731.

Song, J., Klibanov, A. L., Hossack, J. A., & Price, R. J. (2008). Acoustic attenuation by contrast agent microbubbles in superficial tissue markedly diminishes petechiae bioeffects in deep tissue. *Investigative Radiology, 43*(5), 322.

Song, J., Qi, M., Kaul, S., & Price, R. J. (2002). Stimulation of arteriogenesis in skeletal muscle by microbubble destruction with ultrasound. *Circulation*, *106*(12), 1550–1555.

Stride, E. (2009). Physical Principles of Microbubbles for Ultrasound Imaging and Therapy. *Cerebrovascular Diseases*, *27*(2), 1–13.

Talu, E., Powell, R. L., Longo, M. L., & Dayton, P. A. (2008). Needle size and injection rate impact microbubble contrast agent population. *Ultrasound in Medicine and Biology*, *34*(7),

1182–1185.

Taniyama, Y., Morishita, R., Aoki, M., Nakagami, H., Yamamoto, K., Yamazaki, K., Matsumoto, K., et al. (2001). Therapeutic angiogenesis induced by human hepatocyte growth factor gene in rat and rabbit hindlimb ischemia models: preclinical study for treatment of peripheral arterial disease. *Gene Therapy*, *8*(3), 181.

Tran, T.A., Le Guennec, J. Y., Bougnoux, P., Tranquart, F., & Bouakaz, A. (2008). Characterization of cell membrane response to ultrasound activated microbubbles. *Ultrasonics, Ferroelectrics and Frequency Control, IEEE Transactions on*, *55*(1), 43–49.

Treat, L. H., McDannold, N., Vykhodtseva, N., Zhang, Y., Tam, K., & Hynynen, K. (2007). Targeted delivery of doxorubicin to the rat brain at therapeutic levels using MRI-guided focused ultrasound. *International Journal of Cancer*, *121*(4), 901–907.

Tsurumi, Y., Takeshita, S., Chen, D., Kearney, M., Rossow, S. T., Passeri, J., et al. (1996). Direct intramuscular gene transfer of naked DNA encoding vascular endothelial growth factor augments collateral development and tissue perfusion. *Circulation*, 94(12), 3281–3290.

Tu, J., Matula, T. J., Brayman, A. A., & Crum, L. A. (2006). Inertial cavitation dose produced in ex vivo rabbit ear arteries with optison® by 1-mhz pulsed ultrasound. *Ultrasound in Medicine and Biology*, *32*(2), 281–288.

Van Royen, N., Piek, J., Buschmann, I., Hoefer, I., Voskuil, M., & Schaper, W. (2001). Stimulation of arteriogenesis; a new concept for the treatment of arterial occlusive disease. *Cardiovascular Research*, *49*(3), 543.

Van Royen, N., Hoefer, I., Buschmann, I., Heil, M., Kostin, S., Deindl, E., Vogel, S., et al. (2002). Exogenous application of transforming growth factor beta 1 stimulates

arteriogenesis in the peripheral circulation. *The FASEB Journal*, *16*(3), 432–434.

van Wamel, A., Bouakaz, A., Versluis, M., & de Jong, N. (2004a). Micromanipulation of endothelial cells: ultrasound-microbubble-cell interaction. *Ultrasound in Medicine and Biology*, *30*(9), 1255–1258.

van Wamel, A., Bouakaz, A., Versluis, M., & de Jong, N. (2004b). Remote manipulation of cells with ultrasound and microbubbles. *2004 IEEE Ultrasonics Symposium*, *2*.

van Wamel, A., Kooiman, K., Harteveld, M., Emmer, M., ten Cate, F. J., Versluis, M., & de Jong, N. (2006). Vibrating microbubbles poking individual cells: Drug transfer into cells via sonoporation. *Journal of Controlled Release*, *112*(2), 149–155.

Wester, T., Jørgensen, J., Stranden, E., Sandbaek, G., Tjønnfjord, G., Bay, D., Kollerøs, D., et al. (2008). Treatment with autologous bone marrow mononuclear cells in patients with critical lower limb ischaemia. A pilot study. *Scandinavian journal of surgery: SJS: official organ for the Finnish Surgical Society and the Scandinavian Surgical Society*, *97*(1), 56.

Wood, A. J. J., & Hiatt, W. R. (2001). Medical treatment of peripheral arterial disease and claudication. *New England Journal of Medicine*, *344*(21), 1608–1621.

Ylä-Herttuala, S., & Martin, J. F. (2000). Cardiovascular gene therapy. *The Lancet*, *355*(9199), 213–222.

Yoshida, J., Ohmori, K., Takeuchi, H., Shinomiya, K., Namba, T., Kondo, I., Kiyomoto, H., et al. (2005). Treatment of ischemic limbs based on local recruitment of vascular endothelial growth factor-producing inflammatory cells with ultrasonic microbubble destruction. *Journal of the American College of Cardiology*, *46*(5), 899–905.

Zhang, Q., Wang, Z., Ran, H., Fu, X., Li, X., Zheng, Y., et al. (2006). Enhanced gene delivery into skeletal muscles with ultrasound and microbubble techniques. *Academic Radiology*,

13(3), 363–367.

Ziegler, M., Distasi, M., Bills, R., Miller, S., Alloosh, M., Murphy, M., et al. (2010). Marvels, mysteries, and misconceptions of vascular compensation to peripheral artery occlusion. *Microcirculation, 17*(1), 3-20.